Multi-Frequency Processing for Lumen Enhancement with Wideband Intravascular Ultrasound

A Thesis Presented to the Faculty of the

Biomedical Engineering Department

California Polytechnic State University, San Luis Obispo

In Partial Fulfillment of the Requirements for the Degree of

Master of Science in Engineering

By

Rory A. Carrillo

September 2010

COMMITTEE MEMBERSHIP

TITLE:	Multi-Frequency Processing for Lumen Enhancement with Wideband Intravascular Ultrasound
AUTHOR:	Rory Allen Carrillo
DATE SUBMITTED:	September 2010

COMMITTEE CHAIR:	Dr. Lily Laiho
COMMITTEE MEMBER:	Dr. Robert Crockett
COMMITTEE MEMBER:	Dr. Lanny Griffin

Abstract

Multi-Frequency Processing for Lumen Enhancement with Wideband Intravascular Ultrasound

Rory Allen Carrillo

The application of high frequency ultrasound is the key to higher resolution intravascular ultrasound (IVUS) images. The need to further improve the IVUS spatial resolution may drive the transducer center frequency even higher than the current 40 MHz range. However, increasing the center frequency may be challenging as it leads to stronger scattering echoes from blood. The high level of blood scattering echoes may obscure the arterial lumen and make image interpretation difficult. Blood backscatter levels increase with transmission center frequency at a much greater rate compared to arterial tissue. These different frequency dependencies provide a potential method to distinguish blood from tissues by means of multi-frequency processing techniques. To obtain a good blood-tissue contrast with sufficient signal-to-noise ratio, a system with a wider bandwidth is highly desirable. The method described in this paper is based on the ratio of the received signal power between the high (60 MHz) and low (25 MHz) frequency ranges from a novel 40 MHz wideband IVUS catheter. In this paper we will present our in vitro experiment work on porcine blood and a tissue-mimicking arterial wall. Results of multi-frequency processing indicate that blood, at higher frequencies, has a greater backscatter power that is 8X greater than arterial tissue, suggesting this technique will provide a greater contrast between the blood-wall lumen boundary for coronary imaging.

.

Acknowledgements

I would like to thank everyone who supported me through all of my years of college. Thanks to my family: mother, Crissy; father, Ray; sister, Destiney; my best friends Mike, Joe, Dylan, and Bennett; and my Grandmother Elaine for being there every step of the way for me, so that I only had to worry about school, and for always encouraging me to reach higher, even though I didn't think it would be possible.

Thanks to my professors, who have inspired me to continue to learn and grow:

- Dr. Lily Laiho for believing in me, being patient with me, and giving her best guidance throughout this thesis process. I can not thank her enough
- Dr. Wenguang Li, who is one of the most well respected experts in the IVUS industry and is my colleague at Boston Scientific, to whom I cannot express enough appreciation and gratitude. He has supported me and taught me to grow as not only a student, but an engineer.
- Dr. Dan Walsh who believed in me when I applied to the Master's program and transitioned from my bachelor's degree of electrical engineering.
- Dr. Lanny Griffin who has helped me tremendously during my last quarter in school and guided me throughout writing this thesis.

Thanks to Cal Poly, San Luis Obispo, for providing the "learn by doing" environment where students are encouraged to continuously push the envelope and learn concepts outside of the classroom.

I appreciate all of the support and help throughout this research process, and I hope this thesis will be helpful to others in the future.

Rory A. Carrillo

September 2010

Table of Contents

List of Tables

List of Figures

Chapter 1: Introduction

According to the American Heart Association (AHA), in 2004 an estimated 79 million American adults (1 in 3) suffered from Cardiovascular Diseases (CVD) and approximately 871,000 lives were taken. Subsequently, Coronary Heart Disease (CHD) caused 1 of every 5 deaths in the U.S. in 2004. About every 26 seconds, an American will suffer from a coronary attack, and about every minute someone will die from one. CHD is the single largest killer of Americans [1] .

In order to assess the nature of cardiovascular diseases in patients and provide sound feedback on the appropriate therapeutic interventions, it is necessary to develop techniques that are capable of evaluating cardiovascular morphology. Until the end of the 20st century, coronary angiography was the principal method for assessment of the presence and severity for both peripheral and coronary artery disease. However, angiography has several limitations in underestimating the disease severity in vessels due to its silhouette like view of the coronary artery [2;3].

Over the last 20 years, one major minimally invasive diagnostic technique has proven to be capable of defining cardiac morphology and functionality with great accuracy. The technique known as *Intravascular Ultrasound* (IVUS) provides physicians with something other diagnostic techniques do not, higher-resolution tomographic images. However, IVUS does not stand on its own. IVUS can provide physicians with a greater insight into a patient's physiological nature when used in parallel with Angiography.

Intravascular Ultrasound and coronary angiography (also known as X-ray Fluoroscopy) attempt to alleviate the above statistics by combining an imaging modality

that provides high-resolution, accurate cross-sectional measurements of lesion morphology, and a contrast technique to reveal potential lesions within the coronary arteries. Both techniques are combined and necessary in order to properly assess the severity and progression of coronary artery disease in patients, better helping physicians with proper diagnostic evaluations and interventional assessments.

1.1 Background

The following sections will encompass all that is related to Intravascular Ultrasound, including: the circulatory system, coronary arteries, atherosclerosis, coronary artery disease, imaging modalities and their limitations, and finally, the history of Intravascular Ultrasound.

1.1.1 The Circulatory System

The human circulatory system consists of the heart, blood, veins, arteries and capillaries. The main function of the cardiovascular system is to deliver oxygen and nutrients to all tissues in the body and collect metabolic waste. Blood is a carrier for hormones and plays an important role in the immune system. The heart is the muscular organ which pumps blood. The right ventricle pumps deoxygenated blood into the pulmonary arteries, which carry the blood to the lungs, where it passes through a capillary network that enables the release of carbon dioxide and the uptake of oxygen. Oxygenated blood from the lungs returns to the heart via the pulmonary veins, and then flows from the left atrium into the left ventricle, which pumps blood through the aorta, the major artery that supplies blood to the body [4;5].

1.1.2 Coronary Arteries

The arteries that supply the heart muscle, or myocardium, with blood are the coronary arteries. These arteries are capable of maintaining blood flow at levels appropriate to the needs of the myocardium. There are two main coronary arteries; the left coronary artery (LCA) and the right coronary artery (RCA) – see **Figure 1** below. The LCA arises from the aorta and bifurcates into the left anterior descending (LAD) artery and the left circumflex artery (LCX). Coronary arteries have an open space, also known as the lumen, through which blood flows with diameters ranging from 2 to 4 mm [4].

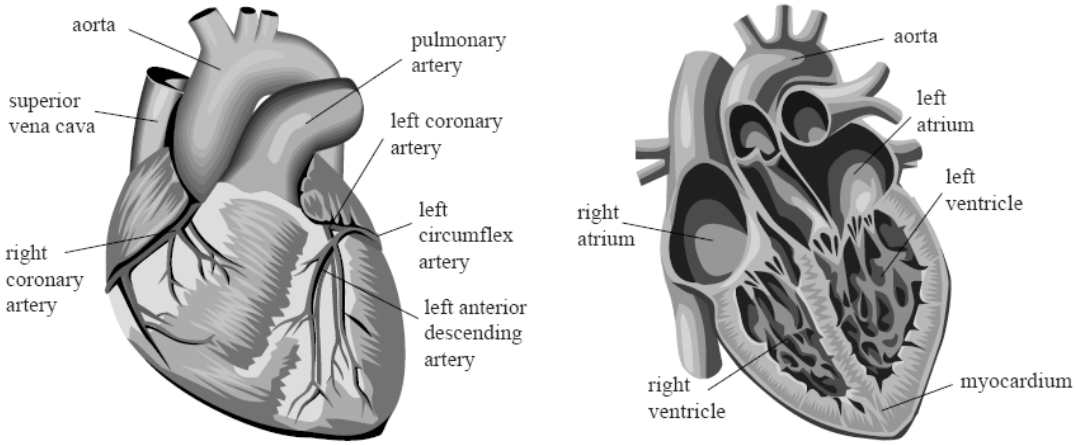

Figure 1: Drawings of coronary arteries and a cross-section of the heart. [Image provided Boston Scientific]

Normal arterial wall consists of three layers: intima, media, and adventitia. The intima is the innermost layer that consists of a permeable endothelial cell layer separating the blood from the vessel wall (roughly 50-150 μm). The internal elastic lamina separates the intima from the media and reduces turbulence of the flow of blood allowing it to be pumped farther. The media, which consist of smooth muscle cells, is the middle layer and

is approximately 200-300 μm and are used to contract or relax the to constrict or dilate the artery to enable blood flow management. The outermost layer, the adventitia, contains smooth muscle cells mixed with fibrous connective tissue and is known to act as a barrier from surrounding tissue.

1.1.3 Atherosclerosis

Atherosclerosis is a disease within the blood vessels. The early atherosclerotic lesion is associated with endothelial cell dysfunction. Cholesterol is delivered by low-density lipoproteins (LDL) through the endothelial cells into the intima, where fatty deposits build up on the inside of the arterial wall [6]. This process causes monocytes, a type of white blood cell, to enter the intima and eventually turn into inflammatory cells called macrophages. Macrophages ingest oxidized cholesterol, delivered by the LDL, and slowly turn into large "foam cells." Foam cells eventually die and further propagate the inflammatory process. Over a period of time, these foam cells develop into atherosclerotic lesions and increase in thickness. These atherosclerotic lesions, also known as plaques, initially expand into the arterial wall [7]. Intracellular micro-calcification deposits form within vascular smooth muscle cells of the surrounding muscular layer, specifically in the muscle cells adjacent to the lesions. In time, as cells die, this leads to extracellular calcium deposits between the muscular wall and outer portion of the atherosclerotic plaques. Plaques within the vessel wall are soft. The progressive plaques consist of fibrotic material or lipids (atheroma), cell debris, calcium crystals and fibrotic material covered by a thin cap (micron range) that has been formed by new connective tissue (fibroatheromas). During the progressive disease process, these

fibroatheromas initially do not restrict the lumen, because of outward remodeling of the vessel. However, in late stages, typically after decades, these fibroatheromas could expand into the lumen, narrowing the opening of the vessel and therefore reduce blood flow. Narrowing of a vessel is called a stenosis. The vasa vasorum are small microvessels within the adventitia of larger arteries (e.g. coronary arteries) that supply the walls of these arteries with nutrients. Vasa vasorum are assumed to play an important role in the generation of atherosclerotic plaque. [8;8]

1.1.4 Coronary Artery Diseases (CAD)

Coronary Artery Disease, a type of CHD, is the result of the accumulation of atheromatous plaques, or atherosclerosis, specifically within the walls of the coronary arteries that supply the muscle of the heart with oxygen and nutrients. The accumulation of plaque on the inner walls of the arteries causes the arteries to harden and narrow; arteries are normally smooth and elastic. As the plaque continues to build up, less blood can flow through the arteries, depriving the heart muscles of the oxygen necessary to function properly, which is called ischemia. Oxygen deprivation to the myocardial muscle fibers can lead to angina (chest pain) or in an extreme case, myocardial infarction (heart attack). **Figure 2** provides an overview of the progress of CAD as described in the previous section (see 1.1.3 Atherosclerosis). According to the American Heart Association in 2007, it was reported that Coronary Artery Disease was the most common type of heart disease and was the leading cause of death in the United States among men and women [1;9].

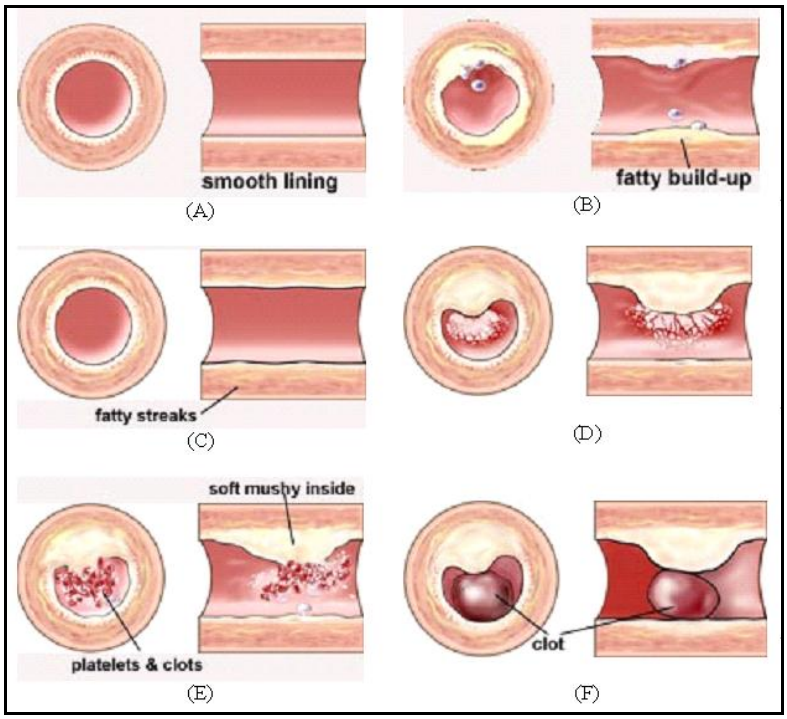

Figure 2: Progress of Coronary Artery Disease

Much effort has been performed in order to minimize CAD. As a result of numerous efforts, many diagnostic methods have been developed to aid physicians in the proper diagnosis of the disease that has and will continue to claim the lives of millions every year [1]. Intravascular Ultrasound and many other imaging modalities have been design to help physicians; however, each has their advantages and disadvantages. Currently, Intravascular Ultrasound has been the leading adjunct technology aiding physicians with determining the severity of diseases such as CAD [10].

1.1.5 Coronary Imaging Techniques

Cardiac catheterization was first described by Forsmann in 1929 [11], and in 1959 it was developed by Sones [12;13], then modified by Judkins in 1967 [14]. Since then, cardiac catheterization has become the technique of choice to assess a patient with

coronary disease. Cardiac catheterization is simply a procedure that examines the blood flow to the heart and tests how well the heart is pumping. During the procedure, a physician inserts a catheter, or a thin plastic tube, into an artery of the arm or leg. From there the catheter is advanced into the chambers of the heart or into the coronary arteries where it can be used to monitor blood pressure, inject a dye for coronary angiography procedures, or even inflate a balloon to open up the arteries (this is known as Coronary Angioplasty). When assessing a patient for CAD, cardiac catheterization remains to be the only clinically accepted method to determine the presence and severity of CAD despite its costs as an estimated 2 million procedures were performed in 2000 [15]. Great strides have been made to enhance the ability to visualize the lumen of the coronary artery but all modalities have their limitations. The following section describes a few of the cardiac imaging modalities used for coronary artery assessment.

Despite the many noninvasive techniques that can be used to help a physician diagnose a patient, the ability to insert a catheter within the vessel still has greater advantages as a diagnostic tool for clinical decision-making as it provides an inside look to what is physiologically occurring within the vessel. The number of catheterizations performed has continued to increase each year, proving to be the diagnostic tool of choice for cardiologists [15].

Coronary Angiography

Coronary angiography is defined as the graphic visualization of the coronary vessels after the injection of contrast media where the images are recorded for future review with X-ray technology [16]. The femoral or brachial arteries are used for catheterization of coronary catheters which distribute the dye, or a contrast media, into

the coronary vessels. The dye (a radio-opaque contrast agent) is visible by X-ray, and as the dye is being injected into the vessel, X-rays are being generated and captured to visually capture on a monitor how the dye is flowing through the vessels of the heart. This typically helps physicians identify and locate where there is an occlusion within the heart. **Figure 3** is a Coronary Angiography, or X-ray image that captures the dye as it flows through the coronary arteries. This X-ray image of the contrast agent within the blood of the coronary arteries allows visualization of the size of the artery lumen. This information allows physicians to determine if a coronary disease is present.

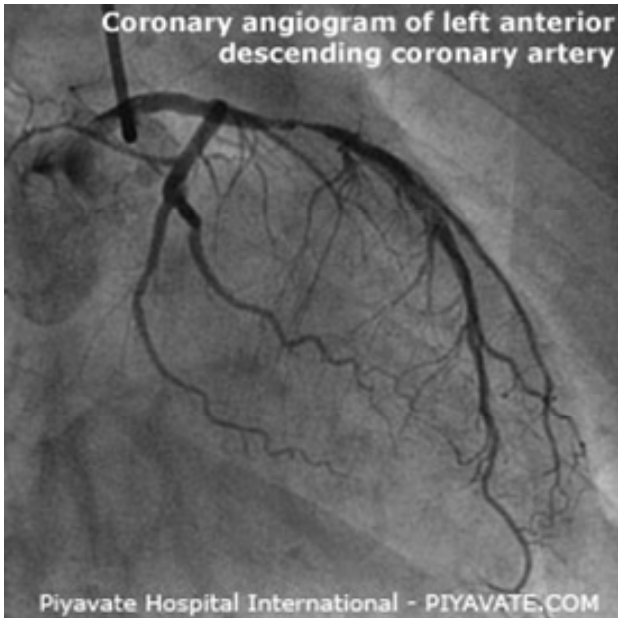

Figure 3: Coronary Angiography Image

The purpose of coronary angiography is to define coronary anatomy and the degree of lumen obstruction of the coronary arteries and remains the standard for providing physicians a vehicle to determine the location of potential coronary disease in a patient [17]. Information obtained from the procedure includes identification of the location, length and diameter of lumen, and contour of the arteries; the presence and

severity of obstruction, characterization of the obstruction (i.e. presence of atheroma, thrombus, dissection etc), and the nature of blood flow. There are three clinical situations in which coronary angiography is used [18]: (1) to determine the presence and severity of CAD in a setting in which the diagnosis is uncertain and CAD cannot be assessed by noninvasive testing such as an echocardiogram or an electrocardiogram, (2) to assess the appropriate form of intervention, such as revascularization or percutaneous surgical intervention, (3) as a research tool for the assessment of treatment results and the progression or regression of CAD [17].

Limitations of Coronary Angiography

Angiography has been the principal clinical tool for determining the severity of luminal stenosis [15;17]; however, considerations regarding the accuracy and reproducibility of coronary angiography are not to be overlooked.

The resolution of modern angiographic equipment, in the clinical setting, is limited to approximately 0.2mm due to the effect of motion artifact, angle of imaging, overlap of vessels, and image display resolution [19]. Other risks associated with this invasive technique include: arterial puncture, iodinated contrast, and radiation. External limitations include multiple staff members, costs, and the long observational period [17]. In 1992, the mean cost for cardiac catheterization for inpatients younger than 65 years was $10,800 which may vary by state [20], but by the year 2000 the average total cost for patients hospitalized for diagnostic cardiac catheterization increased to $16,838 [21].

In clinical practice, the degree of coronary arterial obstruction is expressed as a percent of diameter stenosis. Percent stenosis is done by comparing the diameter of the site of minimum lumen diameter segment to an adjacent segment that seems to be free of

disease and is subject to visual assessment. When luminal narrowings are present on an angiogram, further analysis almost always demonstrates severe obstruction; however, the converse is not true. A normal angiogram does not exclude atherosclerosis, in fact, most studies suggest that coronary angiography underestimates the severity of CAD [22;23]; there are several factors that contribute to this discrepancy.

First, coronary angiography illustrates coronary anatomy from a planar, two-dimensional silhouette of the contrast-filled lumen (see **Figure 3**); however, lesions are often very complex such that one angle of view may misrepresent the severity of narrowing [24]. This can be especially difficult in the left main coronary artery where two orthogonal angiograms may not accurately demonstrate the severity of lesions as these orthogonal views are unobtainable because the stenosis may be obscured by overlapping side branches [25]. **Figure 4** provides an illustration of A) The direction of the X-ray is above a vessel with plaque orthogonal to direction of scan; B) illustrates what the X-ray image would be interpreted as, as if there were no obstructions to the vessel (black color represents contrast agent); however C) illustrates what the image of the vessel would look like if the scan direction was rotated 90 degrees, showing a clear obstruction within the vessel (black being flow of contrast agent, and white being the vessel obstruction).

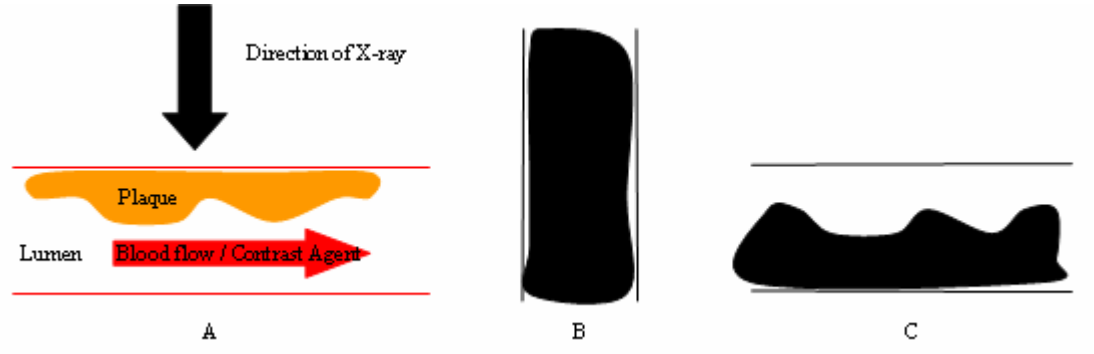

Figure 4: Illustration of Coronary Angiography Limitation: A) represents a vessel with plaque orthogonal to the direction of the X-ray scan. B) Illustrates what the angiography image would look like while X-ray scanning was orthogonal to plaque. (Black fill color represents contrast agent). C) Illustrates what the angiography would represent if the scan direction were rotated 90 degrees (going into the paper), indicated a clear obstruction within the vessel lumen.

Second, coronary "remodeling" may contribute to the inability of coronary angiography to identify mild CAD [2;7;26-28]. Remodeling is a vascular enlargement of plaque during the early stages of plaque accumulation, thereby concealing the atherosclerosis from the angiogram. Once this atheroma becomes severe, the external part of the vessel begins to enlarge, and atherosclerosis becomes evident. These unseen lesions have been reported as a predisposing cause of acute coronary syndromes such as myocardial infarction (MI) [29]. **Figure 5** provides an illustration to depict how coronary remodeling occurs within the vessel walls. In this case, during angiography, plaque build up goes undetected as the contrast agent is able to travel through the vessel lumen unobstructed.

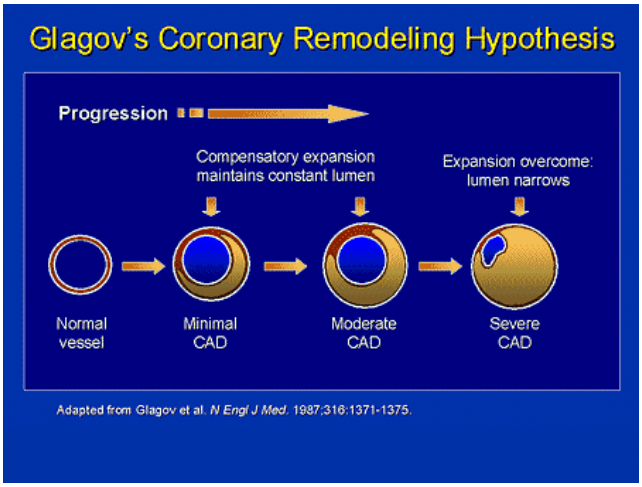

Figure 5: Coronary Remodeling: Coronary remodeling occurs when plaque builds up within the vessel walls rather than within the lumen. Coronary angiography would not capture the disease as the contrast agent would not be restricted from flowing through the lumen.

Third, coronary angiography only visualizes the lumen of the vessel and cannot determine if the wall of the reference segment has CAD [22;30]. In the presence of disease within the reference segment, percent stenosis will underestimate the true amount of lumen narrowing [17;22;30].

These limitations have resulted in the development of new imaging methods to help improve the assessment of CAD. Although these new techniques have not replaced coronary angiography, they have provided additional valuable information that has allowed further assessment of the severity and extent of lumen obstructions. Despite its limitations, angiography still remains as one of the principal clinical tools in the assessment of CAD.

Intravascular Ultrasound (IVUS)

Intravascular Ultrasound is an imaging technique that provides high-resolution, real-time visualization of vessel morphology *in vivo*. Delineation of arterial wall

structures has become imperative in the cardiovascular field, as cardiovascular diseases (CVD) continue to take the lives of millions each year [1]. Despite the prevalence of these diseases, IVUS technology provides imaging methods to properly diagnose and intervene on patients who suffer from a CVD. Such methods include quantitative and qualitative tools for acquiring accurate measurements of cross-sectional dimensions of the arterial lumen [2;28], visualization and assessment of atherosclerotic plaque [2;31], delineation of arterial wall morphology [2], and evaluation of the outcome of an intravascular intervention [2;28]. Overall, IVUS provides a tomographic perspective of lumen geometry and vessel wall structure that other diagnostic imaging techniques cannot.

IVUS is an invasive catheter-based technique that is widely used to assess atherosclerotic plaque [32]. At the tip of an IVUS catheter, a transducer emits an ultrasound pulse and receives the reflected backscatter signal from the tissue where this backscattered signal is then processed real-time into a 2D image. The image permits accurate delineation of the vessel and lumen, dimensions, distribution and severity of coronary plaque [33;34].

An imaging catheter is typically inserted percutaneously into the femoral artery and directed by a guide-wire into the chambers and vessels of the heart (see **Figure 6**). The imaging catheter differs in length and diameter based on the vessel being imaged. At the proximal end of the catheter (end closest to physician), the catheter is connected to a motor-drive unit that is used to spin the drive cable within the catheter sheath. This drive cable is what spins the ultrasound transducer 360° and as the transducer is rotated by the

drive cable at approximately 1800 rpm, the transducer generates and receives ultrasound pulses to and from the coronary tissue.

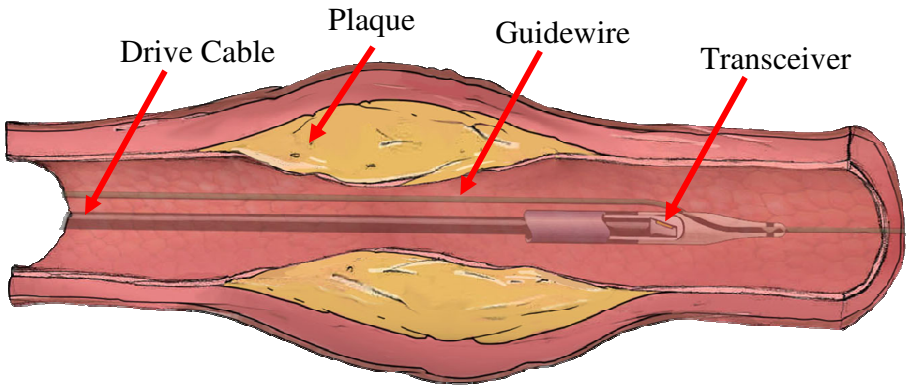

Figure 6: IVUS Catheter in Artery: A mechanical IVUS catheter being pulled back with a coronary vessel to expose vessel morphology. [Image provided by Boston Scientific]

The echoes, or received ultrasound pulses reflected by the tissue, are captured by the transceiver and converted from a mechanical signal (or vibration) to an electrical signal down the drive-cable. The electrical signal is then digitized and rendered onto a display, providing the physician with a 360° cross-sectional view inside the coronary vessel (see **Figure 7**).

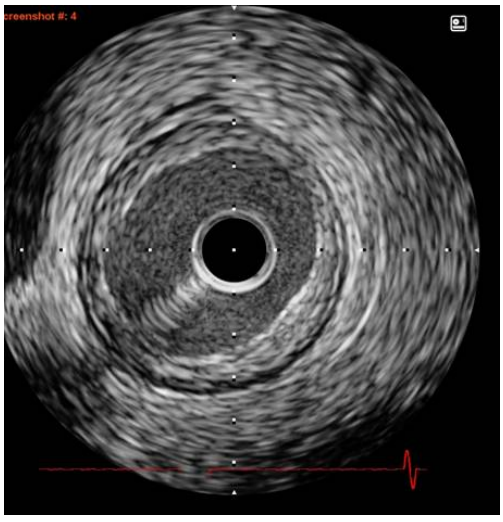

Figure 7: IVUS image: Representation of a standard IVUS gray-scale image providing a 360° view of a coronary vessel. [Image provided by Boston Scientific]

Traditionally, coronary angiography has been used to provide a two-dimensional silhouette of the lumen in coronary vessels to detect the degree and severity of stenosis. Angiography heavily relies on the positioning of the system during imaging, since it only provides a silhouette of the lumen, a physician may be incapable of properly diagnosing he severity of atherosclerosis. Coronary IVUS is most often performed in conjunction with coronary angiography. During an IVUS intervention, arteries as small in diameter as 1.5 mm can typically be visualized and typically the patient is given intravenous heparin and intracoronary nitroglycerin which prevents blood coagulation within these small coronary arteries. The procedure is typically performed by a cardiologist or interventional cardiologist in a cardiac catheterization laboratory. IVUS imaging provides a tomographic 360-degree sagittal scan of the vessel media (blood) to the vessel wall. IVUS measurements of arterial dimensions (minimal and maximal diameters, cross-sectional area, and plaque area) complement and enhance angiographic information. When a mechanical pullback of the IVUS catheter is performed at a fixed rate, a three-dimensional (3D) reconstruction of the artery can be obtained [35;36]. More details on how IVUS works will be discussed in a later section.

Limitations of IVUS

As is the case with all technologies, there are limitations. One of the biggest setbacks with IVUS technology is image interpretation. The technician studying the images needs a solid understanding of the potential ultrasound artifacts. Generally, artifacts are easily recognized, but in some cases artifacts may adversely affect the image quality, and ultimately increase the difficulty of interpretation and reduce the accuracy of the quantitative measurements [23;37].

Artifacts are structures and features on an image that do not have a one-to-one correlation to the object being scanned. Non-uniform rotational distortion (NURD), ring-down and geometric distortion are common artifacts that make image interpretation difficult. NURD is only found in mechanical systems (explained later) and is caused by uneven mechanical drag on the catheter drive shaft that results in cyclical oscillations in rotational speed. Ring-down is a phenomenon that occurs immediately around the catheter and results in bright circular areas in the image that can interfere with image interpretation when the transducer is close to the arterial wall. Geometric distortion results from imaging in an oblique plan, creating an elliptical, rather than circular, cross-sectional image.

Another major limitation of IVUS is its low specificity for the diagnosis of a thrombus. A thrombus, or blood clot, occurs when blood vessels are damaged and cause platelets to adhere to the damaged endothelial cells; in most cases, the formation of a clot is due to ruptured plaque. The formation of a thrombus on top of ruptured plaque is considered to be a sign of an acute coronary syndrome and the use of IVUS to determine the amount of clot contributing to a stenosis would greatly assist in clinical decision making [23;38-40;40]. The limitation is due to the fact that a thrombus, under IVUS image interpretation, looks similar to plaque tissue therefore making it difficult to differentiate.

Optical Coherence Tomography (OCT)

OCT is similar to Intravascular Ultrasound (described later) but instead of acoustic waves, a light source is emitted towards the sample [41]. The time delay information and intensity of backscatter of light from the varying internal structures vary

with optical properties. Because the speed of light is so fast, OCT uses a technique called low-coherence interferometry, where light reflected back from the sample is measured by correlating it with light that has travelled a known reference length. OCT uses near infrared light, ~1300 nm, because light with a shorter wavelength is prone to a higher degree of scattering and absorption, while light with a longer wavelength results in undesirable absorption attenuation. With OCT, a spatial resolution of 4 to 16 μm is achieved with a penetration depth of 2 to 3 mm. [42-44]

Limitations

One of the major limitations for OCT is that it requires a blood-free zone for imaging that is accomplished by a saline flush or an occluding balloon. This is because light is significantly absorbed and scattered by blood cells, which degrades the coherence and image quality. Overall, it is a cumbersome procedure compared with other imaging modalities [42-44]. Another limitation of OCT is that its depth range is limited to approximately 3-4mm and depth penetration in tissue is limited to 1-3 mm, which limits imaging beyond the internal elastic lamina [42-44]. Additionally, stent struts appear as bright local reflections with shadowing sectors radially behind them, which gives the tendency for OCT to underestimate the stent strut thickness in reference to manufacturers' specifications especially when blood is present [45]. Despite its limitations, studies demonstrate the feasibility of cardiac OCT to visualize coronary disease in patients [42-44].

1.1.6 History of Intravascular Ultrasound

The start of ultrasound technology first began in 1880, where Paul and Jacques Curie discovered that in some materials (notably crystals) an electric potential is generated in response to mechanical stress (deformation); this technology was given the name *piezoelectricity*. Similarly, the reverse was found true [46]. Consequently, subsequent discoveries were made that led Sokolov to believe ultrasound could be used for the detection of flaws in materials [47-49]. Later, in 1937, Sokolov was awarded a patent for his ultrasound flaw-detection device [48]. It was not until 1942 an attempt was reported on using ultrasound as a diagnostic tool. However, Meyer reports of earlier applications of ultrasound for use in medical therapeutics [49].

Neurologist Dr. Karl Dussik of Vienna, Austria, was the first to attempt to use ultrasound as a diagnostic tool in 1942 [49;50]. Dussik's attempt was based on the *transmission method*, where a sample (in this case the skull) was exposed to a beam of ultrasonic rays by one transducer and recorded by another on the opposite side of the sample. The changes in attenuation that traversed through the sample were recorded on an oscilloscope. In 1952, Guttner et al. determined that the transmission method was of no value due to the absorption and reflection of the bones within the cranium [50] and another method was soon reported, known as the *reflection method*.

In 1949, Ludwig and Struthers attempted to use the reflection method to detect gallstones and other foreign elements deep within the muscle of dogs [50]. The reflection technique is where both the transmitter and receiver are located on the same side of the sample under examination. Sound pulses are emitted for long intervals, where a fraction of the sound is reflected by tissues with different densities – every kind of tissue has

characteristic impedance that makes its reflection distinguishable. The reflected pulses, or echoes, are recorded on an oscilloscope.

The development of ultrasound as a medical diagnostic and therapeutic tool in cardiology began in the early 1950's. Inge Edler, a cardiologist, and Carl Helmuth Hertz, a physicist, collaborated together to see if ultrasound technology could be used to examine the heart. Their first work entailed using a sonar device, or reflectoscope, to record echoes from Hertz's own heart [49]. However, as is the case with most technologies, the rise of ultrasound in cardiology evolved from other applications of ultrasound, as it was Edler's job to evaluate cardiac patients prior to heart surgery [51]. Simultaneously, researchers such as Dr. Wild and Dr. Reid from the United States began ultrasound studies on the human heart [47;52].

In 1966, 10 years after Wild and Reid first began studying the heart, Kossoff described a catheter tip transducer of 2mm in diameter operating at 8 MHz for measuring ventricular wall thickness [53]. A few years later, a group applied a 2.5 MHz cylindrical element that radiated through a 360° arc [54]. At the same time, Stegall et al. introduced two transducers mounted at the end of a catheter to determine the intra-aortic and intra-carotid diameter [55]. However, it was Wells, in 1966, who first came up with a practical design using an intravenous probe with mechanical rotation and a flexible shaft for rotational real-time cross-sectional imaging [56]. But despite all these advancements in intravascular ultrasound, there were many limitations that made IVUS imaging impractical for clinical use such as not being able to conduct real-time analysis. Thus, Bom et al set out to develop invasive real-time and cross-sectional ultrasonic imaging using state-of-the-art technology. His group developed a 32-element circular phased array

mounted on the tip of a catheter to record real-time intra-luminal images of ventricles in animals; however, the catheter size and steerability provided serious limitations [57].

The simplest approach has been circumferential scanning with a single transducer to provide cross-sectional imaging through the blood of the arterial wall under the endothelial surface. The mechanical single-element design was investigated by many groups and chosen over the electronic multi-element system as described by Bom. The electronic multi-element phased array ultrasonic catheter allowed for a reduction in the number of electrical wires, thus, a smaller size catheter with greater flexibility. However, the main problem with the phased-array technology is that it was complicated and expensive. Resolution and artifacts in the near field put limitations on the technology for smaller diameter vessels and stenosis. These complications made the single-element design much more attractive. The single-element is a design where the transducer was mounted in the axis of the catheter where the ultrasound can be swept around in a plane perpendicular to the catheter's long axis by rotating the transducer (in a manner similar to a lighthouse) to obtain a 360° display of the arterial cross-section. This technology was great for imaging small arteries (i.e. coronary arteries) as the single transducer at high frequencies (>20 MHz) had great attenuation with distance. [58]

Chapter 2: Basic Principles of Ultrasound

In order to gain a greater understanding of the fundamentals for intravascular ultrasound imaging, it is necessary to review some of the physical mechanisms that relate to ultrasound and using ultrasound for coronary imaging. The following section provides a survey of mechanical and acoustic principles for ultrasound imaging.

2.1 General

Sound can be described as a mechanical energy that propagates through a medium, these are called – *pressure waves.* Ultrasound is defined as sound waves with frequencies above the upper limit of human hearing of 20 kHz. Ultrasound imaging is based on the reflection method (or pulse-echo method as described previously), where a short ultrasound pulse is transmitted and received by the same source (transducer) that converts electrical energy into acoustic energy, and vice versa. In the application of IVUS, the transmitted ultrasound pulses travel through various coronary tissue and are scattered, reflected and refracted at tissue boundaries. The scattered and reflected ultrasound waves are called *echoes*; the receiver detects the acoustic vibrations and converts the vibrations pulses back into electric signals for the IVUS system to interpret. Although there are many diagnostic ultrasound applications, cardiology is one of the few fields that use high frequency (>10 MHz) ultrasound as a diagnostic tool.

Before discussing the in-depth details of Intravascular Ultrasound, it is necessary to discuss some of the fundamental concepts of ultrasound physics. This next section (Sec 2.2) is for novice readers and may be skipped by those who are familiar with the basic concepts of ultrasound physics.

2.2 Ultrasound Waves

Unlike most of the waves we encounter on a daily basis, ultrasound waves are longitudinal mechanical waves that propagate at a frequency greater than 20 kHz – beyond the range of human hearing. Mechanical waves are such that they need a medium for propagation, unlike electromagnetic waves that travel at the speed of light and do not need a medium to propagate. Mechanical waves travel through deformable, elastic mediums as the energy of the wave causes displacement of the medium particles. The energy in the mechanical waves is transmitted through the motion of the particles, where the medium itself does not move from one place to another. In other words, ultrasound is the transmission of mechanical vibrations through a medium.

Mechanical waves are categorized as either longitudinal or transverse, which correlates to the direction of the displacement of the individual particles of the medium. All acoustic waves are longitudinal, where the particles in the medium move parallel to the direction of the wave; conversely, transverse waves cause particles to displace perpendicular to the direction of the wave. To visualize how an ultrasound wave propagates, imagine the individual particles are connected to each other by springs. An incident wave will cause the first particle to compress the spring between the first and second particle. This *compression* energy is then transferred between particles two and three and particles one and two undergo what is called *rarefaction*, this is a result of each particle oscillating about its equilibrium point every time a wave passes [59].

2.2.1 Frequency

Describing the temporal behavior of a sound wave is useful when modeling ultrasound waves. The description of compression and rarefaction above will give us something similar to a sine wave if we were to plot pressure versus time. Think of acoustic pressure the same as atmospheric pressure. During compression, the acoustic pressure is elevated above atmospheric pressure, and during rarefaction, the acoustic pressure corresponds to where the pressure is lower than atmospheric pressure. The resultant number of times per second either compression or rarefaction occurs at any point is called *frequency*. The frequency of a sound wave is determined by the number of oscillations per second made by the sound wave (e.g. sine wave).

The time it takes for the wave to complete a cycle is called the *period*. Period (T) and frequency (f) are inversely related as shown [60-62]:

$$T = \frac{1}{f} \qquad 1$$

2.2.2 Characteristics of Ultrasound

The propagation speed c of sound waves in a medium is determined by its bulk modulus E and density ρ, where a more dense material has a greater the speed of sound [60-62]:

$$c = \sqrt{\frac{E}{\rho}} \qquad 2$$

The Intensity *I* of a sound wave, of the flow of energy through the unit area at a point is related to the pressure amplitude *p* by [60-62]:

$$I = \frac{p^2}{2\rho c} \qquad 3$$

The physical property of a medium which determines the reflection of sound waves is its acoustic impedance *Z*, the product of propagation velocity *c* and density *ρ* [60-62]:

$$Z = c\rho \qquad 4$$

The wavelength λ, the distance between two consecutive points of equal pressure, is related to the frequency *f* and the propagation speed *c* as follows [60-62]:

$$\lambda = \frac{c}{v} \qquad 5$$

For a given medium, the higher the frequency the smaller the wavelength will be. The propagation of a sound wave in tissue is influenced by physical effects of which the most important are reflection, refraction, scattering, and absorption.

2.2.3 Reflection and Refraction

As a sound wave passes from one medium to another with different acoustic impedances, a part of the incident wave is reflected at the boundary and a part is transmitted through to the second medium, generally with an altered direction of propagation, better known as refraction.

The angle of the reflected wave is equal to the angle of the incident wave. The angle of the refracted wave depends on the velocities of sound in the first and second media, which is given by Snell's law [60-62]:

$$\frac{\sin\theta_1}{\sin\theta_2} = \frac{c_1}{c_2} \qquad 6$$

The ultrasound speeds in biological soft tissues are very similar and there is only a little deviation from the direction of the incident wave, which may be ignored.

The reflection coefficient R, the ratio for the reflected intensity I_R and the incident intensity I_I, is determined by the acoustic impedances Z_1, Z_2 of the two media, the incident angle, and the angle of refraction [60-62]:

$$R = \frac{\left(z_2\cos\theta_1 - z_1\cos\theta_2\right)^2}{\left(z_2\cos\theta_1 + z_1\cos\theta_2\right)^2} \qquad 7$$

In the case where the incident wave is normal to the boundary, where $\theta_1 = 0°$, the calculation of the reflection coefficient R is much simpler [60-62]:

$$R = \frac{\left(z_2 = z_1\right)^2}{\left(z_2 + z_1\right)^2} \qquad 8$$

The acoustic impedances of different soft tissues are slightly different, such that the reflection coefficient is very small. At boundaries between soft tissue and bone or air, a substantial part of the incident energy is reflected. Reflection and refraction describe the phenomena at smooth boundaries with large dimensions compared to the wavelength. If the boundary is not smooth, parts of the incident wave is reflected in different directions, so in addition to the directed specular reflection (e.g. mirror) there is non-directional reflection.

2.2.4 Scattering

If a sound wave strikes a boundary layer that is not smooth, where the dimensions are comparable with or smaller than the wavelength, then part of the intensity of the wave is scattered in all directions. The discontinuities at the boundary layer are local changes in compressibility, density, or even both. The scattered parts of the wave resulting from the randomly distributed scatters may superimpose. Thus, there may be an enhancement of the intensity or the waves may cancel. Tissue is a grainy medium and because it is composed of cells, the scattering of the grainy medium is the reason why the homogenous regions of tissue show a “speckle” structure in ultrasound images.

2.2.5 Absorption and Attenuation

Scattering and reflection of a sound wave propagating in tissue is not the main reason for loss of energy; absorption is another primary factor in the loss of energy of sound waves. The mechanical energy of the wave is transformed into heat which is dissipated within the medium. The absorption depends on the medium and strongly increases with frequencies in the frequency range used in medical diagnosis. The exponential laws describe the amplitude A and the intensity I of the wave on the traveled distance [60-62]:

$$A = A_o e^{-(\gamma s)} \qquad 9$$

$$I = I_o e^{-(2\gamma s)} \qquad 10$$

The absorption (attenuation) coefficient γ is in units dB/cm. Blood is known to have an attenuation coefficient of 0.2 dB/cm at 1 MHz [58] – This value changes as the frequency changes nonlinearly with frequency.

2.3 Ultrasound Transducer Properties

As mentioned previously, in general, a transducer refers to a device that converts signals or energy from one form to another. Ultrasound transducers are used to convert acoustic energy to electrical signals and electrical signals to acoustic energy; they are used to detect and transmit ultrasound waves.

Transducers used for medical ultrasound imaging employ the piezoelectric effect to generate and detect sound waves (as described in Chapter 1). There are a number of piezoelectric materials such as quartz that are used for diagnostic ultrasound, but lead zirconate titanate (PZT) is the most common ceramic used in ultrasound imaging [61]. These materials must be polarized before they can transmit and receive sound waves effectively. This is done by heating the material above 36.5° C, for PZT, and then applying a high voltage across the material to align the crystals, which is also known as polarization. The material is then cooled with the voltage still applied as this will allow the material to maintain polarization, giving it the desired piezoelectric properties [61].

The speed of sound and thickness of a piezoelectric material determine its center frequency. Transducers are also characterized by their transmit and receive sensitivity, both as a function of frequency. The center frequency and bandwidth determine the pulse length of the transducer. A transducer that is sensitive over a wide range (high bandwidth) of frequencies can transmit short, broadband pulses. These properties are essential is determining a transducers' spatial resolution and will ultimately effect image quality.

2.3.1 Solid-State vs. Mechanical Transducer Elements

A 360° cross-sectional tomographic image is produced with a variety of technologies. Solid-state technology uses a circular multi-element phased-array of transducer elements on the tip of a catheter (see **Figure 8**). The image is created by sequentially firing the array of transducers, and simultaneously receiving echoes by programming one set of transducers to transmit and another to receive.

Mechanical technology uses a single element transducer located at the tip of a catheter (see **Figure 8**). The transducer is rotated mechanically via a flexible drive shaft connected to a drive motor. The transducer transmits and receives ultrasound signals at approximately 1.5° increments to create the tomographic image. The transducer element provides 256 vectors, or scan lines, for each image. The motor drive at the end of the catheter facilitates uniform mechanical pullback of the transducer within a protective sheath. The experiments performed in this thesis used the single element mechanical technology just described.

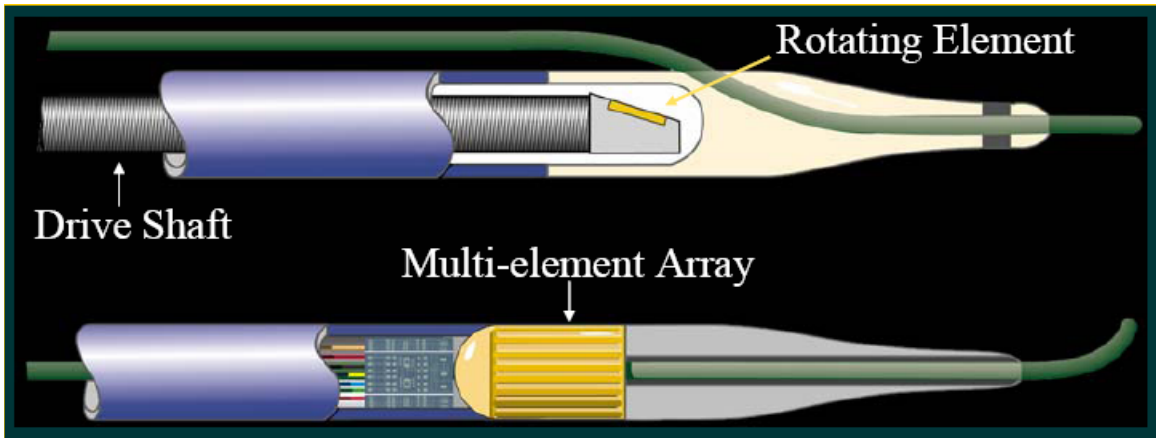

Figure 8: Multi-element and single element technologies [Image provided by Boston Scientific]

2.3.2 Resolution

Due to its ability to provide detailed *in vivo* images of coronary vessels, IVUS has assumed the role in the diagnosis and treatment of coronary artery diseases. As IVUS technology progressed, a wide array of systems, catheters, and transducers have been developed to provide enhanced image quality. IVUS image quality is especially important in that detecting the small differences may play an important role in identifying

vulnerable plaque in a vessel or determining the outcome of specific therapy. There are many key players in IVUS that enhance the quality of the system overall; these basic principles are what drive the success of an intravascular ultrasound system, and the main component being the transducer as it drives the resolution capability of the entire system.

Spatial Resolution

Optimizing resolution is one of the most important elements in an ultrasound system; the better the resolution, the better the image quality (i.e. clarity). Resolution is the minimum distance two targets can be distinguished on a display. There are two types of resolutions important to ultrasound imaging: *axial* and *lateral* resolution, both of which are directly related to the transmission frequency and transducer used and are key elements in the image quality for IVUS.

Axial Resolution

Axial resolution is the resolution along the axis of the ultrasound beam, and is determined by the pulse length (determined by transducer frequency and bandwidth) - the shorter the pulse length (i.e. higher the frequency), the greater the resolution and is described by the following:

$$\text{Axial Resolution} = \text{spatial pulse length (SPL)} / 2$$

$$\text{Where SPL} = \lambda \times \text{no. of cycles}$$

The axial resolution of a transducer is generally better than its lateral resolution, where the axial resolution for a 20 MHz transducer is 200 microns and approximately 100 microns for a 40 MHz transducer [58]. **Figure 9** provides a visual diagram to help better understand this characteristic. Axial resolution is dependent on the pulse length. Because the ultrasound pulse is small enough in this example, the transducer will pick up two reflections. As the scattering elements approach each other, the pulse becomes longer in comparison, thus only one reflection will be seen by the system.

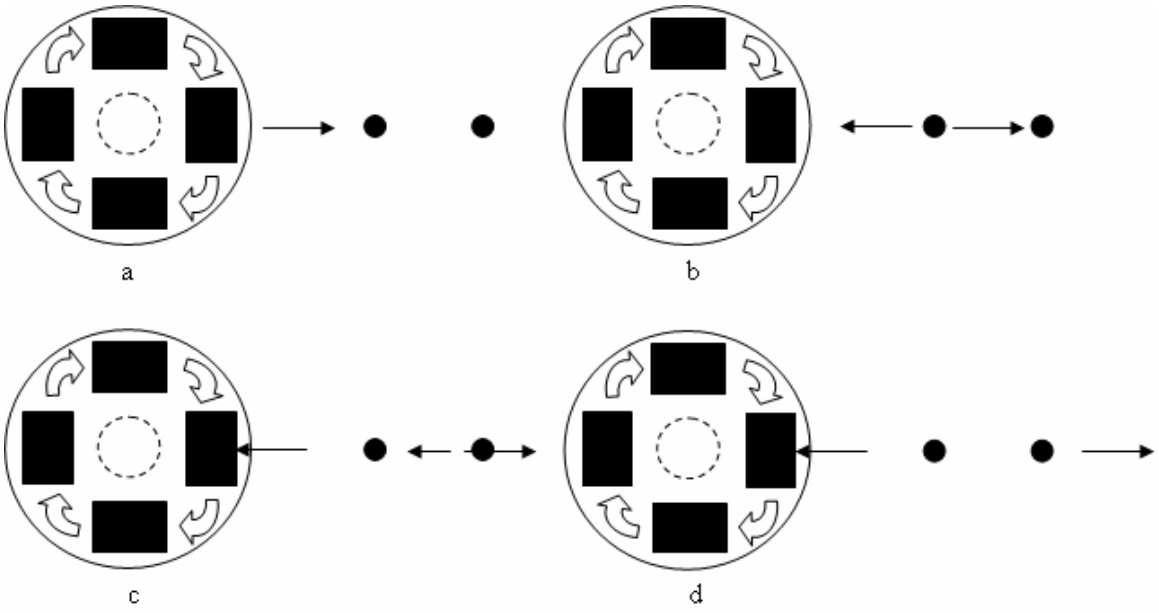

Figure 9: Axial Resolution Representation The black box represents the transceiver element rotating 360° within the catheter. The scattering elements are the black, small and round dots. A) Represents the ultrasound signal (US) being emitted from the transceiver traveling towards the scattering element. The US spatial pulse length is represented byt eh magnitude or length of the black arrows. B) As the US hits the first scatterer, a portion of the US is reflected back to the transceiver while another portion is transmitted through the element towards the next element. C) The first reflected US hits the transceiver while the second reflected US begins traveling towards the transceiver. D) The final reflection from the second scatterer reaches the transceiver at a time after the first, enabling the transceiver to differentiate between both reflections. Axial resolution is dependent on the pulse length. Because the ultrasound pulse is small enough in this example, the transducer will pick up two reflections. As the scattering elements approach each other, the pulse becomes longer in comparison, thus only one reflection will be seen by the system.

Lateral Resolution

Lateral resolution can be described as the resolution perpendicular to the beam axis and is directly related to the beam cross-section (See **Figure 10**). Said differently, it is the ability to distinguish adjacent targets perpendicular to the ultrasound beam. Lateral resolution is determined by the geometry of the transducer (the diameter) and transmission frequency. Basically, two objects side by side (see **Figure 10**) cannot be distinguished if they are separated by less than the beam width of the transceiver. The determinants of beam width are transducer frequency where beam width increases with lower frequency transducers and vice verse. We already know that resolution increases with frequency, however, attenuation of the ultrasound wave increases as the frequency increases, and as a result, the penetration depth is limited. This is due to the US wave becoming smaller in wavelength, making it unable to penetrate elements that are bigger than the wavelength itself. Consequently, non-invasive ultrasound imaging is performed at 1-5 MHz in order to optimize the penetration depth [63]. High frequency ultrasound applications (>10 MHz) have penetration depths of <1.5cm, but have higher resolutions (<200 μm). Typical 40 MHz IVUS transducers provide approximately 0.5 mm of lateral resolution [58].

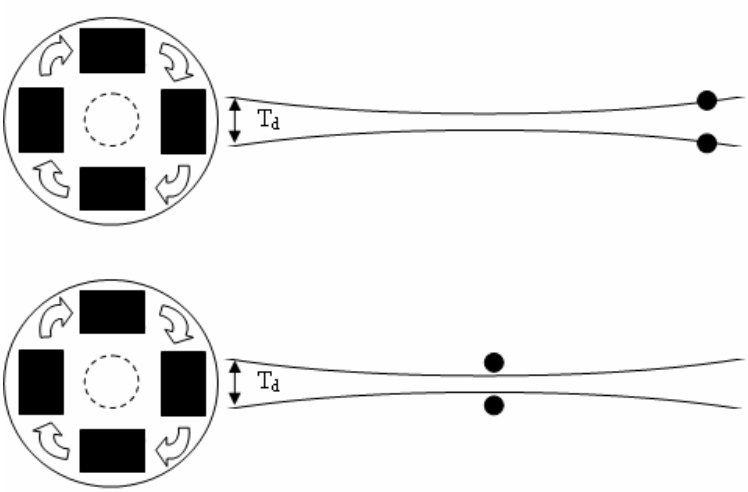

Figure 10: Lateral Resolution Diagram This illustration shows that the beam width, or diameter of the transducer, determines the lateral resolution. The smaller the beam width, the more capable a ultrasound system can differentiate between two elements. Also, due to beam spreading, once the scattering element is beyond the focal point, lateral resolution begins to worsen as shown. This can only be improved by decreasing the size of the transducer itself.

2.4 Intravascular Ultrasound System

A typical IVUS system consists of six main components as shown in the schematic below (see **Figure 11**): Catheter, motor drive unit, transmitter, receiver, signal processing module, and the display. The ultrasound transducer sits at the tip of the catheter. As described previously, the motor drive unit rotates the drive cable that the transducer sits on at 1800 rpm.

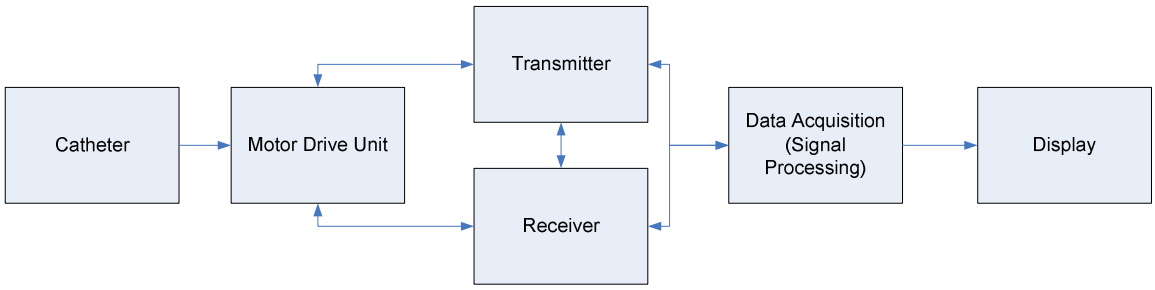

Figure 11: Basic IVUS System Block Diagram

The transmitter generates short voltage pulses that are applied to the piezoelectric crystal in the transducer. The amplitude and frequency of the pulse can be adjusted with the system where a typical excitation pulse ranges from 50 – 100 V, with frequencies ranging from 10 – 40 MHz.

The receiver amplifies the small voltage signals that are returning echoes from the tissue striking the transducer. Because ultrasound is attenuated as it travels through tissue, and because some scaterrer elements are further away than others, a time-dependent amplification, generally called time-gain compensation (TGC), is used to compensate for the attenuation loss and time delay. Attenuation occurs as an US signal penetrates scatterers (i.e. blood and tissue) causing some of the US energy to be reflected in different directions and never being detected by the transceiver. Filters and a master gain control are also used for noise reduction and global amplification if needed.

Because the human eye can only distinguish about 200 different gray levels, the received echo signal is compressed by an adjustable logarithmic amplifier to avoid a loss of information when transformed into a video image – the dynamic range of the received signal is about 50 dB [58;61]. At the same time, the high frequency echo signal is demodulated to obtain an enveloped signal, or an intensity signal. Once this occurs, the intensity signal is then scan converted. Scan conversion is necessary because scanning of the vessel cross-section creates a series of intensity scan lines that have to be transformed for a 360° geometrical display. Closer to the transducer these scan lines may overlap, therefore, during scan conversion the intensity of pixels close to the transducer is calculated by averaging over several scan lines. Averaging over several images may

reduce image noise and may be used to increase image quality. Finally, the signal processed intensity signal is displayed on the video monitor.

2.5 Physical Properties of Tissue Relevant to IVUS

Although IVUS has proven to be a highly accurate imaging modality, widely used as a complimentary diagnostic tool to angiography, much of the research today is focused on methods of continuing to improve upon resolution and image quality. The focus of this study was to determine the feasibility of improving upon the blood-tissue boundary by using a multi-frequency enhancement method. Blood has shown to be frequency dependent, whereas tissue has not - perhaps this is due to the increase in the size of the scattering element [64]. Thus, understanding the physical and acoustic properties of both the blood and vascular tissue are of importance. The following sections will outline the results of previous studies on the physical and acoustic properties for both blood and arterial tissue.

2.5.1 Properties of Arterial Tissue

Mechanical Properties

There are three layers of an artery: the intima, media, and adventitia. The intima consists of the endothelium, which is a single-cell layer of connective tissue that encounters the blood within the artery. The media consists of smooth muscle layers composed of elastin and collagen fibers. The adventitia is composed of mostly collagen fibers. Thus, arteries are multi-layered anisotropic structures that are pre-stressed

longitudinally and circumferentially based on the orientation of the smooth muscle in each layer. Additional mechanical and acoustic properties relevant to this study are discussed further in the following sections.

Acoustic Properties

As with any media, ultrasound propagation through the artery results in attenuation and distortion of the ultrasound beam by refraction and diffraction. According to Duck [65], the speed of sound for whole arteries was found to be 1616 cm/s. This was verified by Saijo et al who reported an average velocity of 1619 ± 42 m/s [66]. Due to the physics of ultrasound, as the media in which the ultrasound is propagating in becomes more dense, the beam will propagate faster through the media. This incident was observed by Rooney et al as they report a velocity as high as 2000 m/s in diseases arteries with high level of collagen and cholesterol [67]. Attenuation in the arteries has been reported by [67-69]. The average attenuation for all three layers of the artery is 11 ± 4 db/cm/MHz, higher in calcified regions, and lower in lipid regions.

Lockwood reported on the acoustic backscatter derived from arterial tissues [70], but these were not within the coronary vessels. Lockwood and other authors report that the acoustic backscatter measurements in the arteries have demonstrated higher backscatter in regions of calcification and fibrous plague compared to healthy arteries. However, none of which conclude that arterial tissue is frequency dependent.

2.5.2 Properties of Blood

Intravascular ultrasound has become a valuable diagnostic tool in interventional cardiology, providing physicians with detailed, high quality, cross-sectional images of vessels. However, resolution and image quality are the primary focus of research. As described previously, resolution enhances the discrimination between various biological tissues. Therefore, as the resolution increases, the image quality increases where the resolution of an imaging system greatly depends on the center frequency of the transducer. As the frequency increases, the axial resolution increases because it is determined by the length of the ultrasound pulse, which means, the shorter the pulse length, the greater the axial resolution. However, as the frequency increases, studies have noticed that there is a strong blood backscatter (echo) signal that makes blood appear like tissue, which may cause difficulties in the discrimination between the lumen and arterial wall boundaries [64;70;71]. Additionally, there are many other factors that may affect the echogenicity, or the tendency of tissue to reflect ultrasound, of blood backscatter. Researchers have reported that the hemodynamic and hematological factors such as hematocrit, protein concentrations, and blood flow dynamics [72;72-75] affect the echogenicity of blood; thus, the properties of scattering in blood should be well understood. In the following section, blood as a medium in ultrasound will be given.

Physical Properties

Blood is composed of liquid called plasma where erythrocytes (red blood cells), leukocytes (white blood cells), and platelets are suspended. Erythrocytes are elastic, nonnucleated bioconcave disks with an average diameter of 7μm and a thickness of 2μm

[76;77]. The number of red blood cells is significantly larger than that of white cells and the volume of a red cell is much larger than that of a platelet [77]. Thus, scattering of ultrasound by blood is presumably due to red blood cells [76].

Mechanical Properties

Blood is non-Newtonian and is shear-thinning, such that the viscosity of blood decreases with an increase in shear rate [77]. The shear thinning properties of blood is known to be a result of changes in the aggregation and deformation behavior of the red cells [78]. At low shear rates, the red cells form *rouleaux*, in which the red cells join base to base, creating an interlocking structure so that the blood resembles a solid – essentially increasing the scatterer size and ultimately the echo intensity. An increase in shear rate breaks down the "bridging" between cells and reduces the rouleaux length, thus the number of individual blood cells increase. A study has shown that for shear rate in the range 0 to 1 s^{-1}, aggregation dominates the viscous behavior, whereas in the range 1 to 100 s^{-1}, deformation is the dominant factor [79].

Acoustic Properties

The backscatter signal from blood arises from the scattering elements that are individual red blood cells and red cell aggregates, called *rouleaux*. For scatterers small with respect to wavelength, there is Rayleigh scattering with dependence on transmit frequency, f, of f^4, whereas scatterers large with respect to the wavelength show no dependence on transmit frequency [80]. A frequency dependence of $f^{3.5}$ in whole human blood at a shear rate of 32 s^{-1} at 40 to 60 MHz was found by Foster [64]. A lower

frequency dependence occurs where aggregation is expected because of the larger size of the scattering particles [64;74]. Other factors such as red cell volume [81], transmit frequency [82], shear rate [74;83;84], hematocrit [84-86], fibrinogen concentration [82;87;88], turbulence [85], angle [89]and cycle length all influence the backscatter signal from blood. Fontaine et al. concluded that the main determinant in backscatter power is red cell aggregation [72]. Understanding these properties will provide a better understanding when trying to differentiate between red blood cells and arterial tissue during IVUS imaging.

2.5.3 Blood versus Arterial Tissue

The purpose of this study is to determine the feasibility of using a multi-frequency processing method to differentiate between blood and arterial wall, which will ultimately enable us to delineate the blood-tissue boundary and assess the degree of lumen reduction for atherosclerosis.

First, in 1991, Lockwood reported that blood, at high frequencies (25-65Mhz) "was found to produce scattering that was within an order of magnitude of what was measured in some vascular tissues" [70]. Then, in 1994, Foster reported that at low shear rates and high frequency, the backscatter power from blood was comparable with the backscatter from the tissue media [64]. The force to improve upon image quality will lead to higher frequency imaging, and as Foster and Lockwood found, the frequency dependency of blood could increase the contrast on IVUS images where the discrimination of the blood-wall lumen would not be as easy to delineate compared with lower frequencies. The following experiment was designed in such a way as to determine

the feasibility of a method to increase the contrast between the blood-wall lumen boundary that is substantially grounded on the premises of prior studies.

Chapter 3: Multi-Frequency Processing for Lumen Enhancement

3.1 Overview

The use of high frequency ultrasound is the key to obtaining higher resolution IVUS images. As stated previously, the greater the transducers' center frequency, the greater the image resolution. Consequently, increasing the transducer center frequency beyond that of the standard 40 MHz may introduce some challenges from stronger scattering intensities from blood as reported in the previous section by Foster [64] and Lockwood [70]. This high level of blood scattering may obscure the arterial lumen and make image interpretation difficult for physicians [90]. However, frequency dependency by blood may provide the potential to distinguish blood from tissue by means of multi-frequency processing techniques. In order to obtain a good blood-tissue contrast with sufficient signal-to-noise ratio, a system with a wider bandwidth is desirable. The proposed method is based on the Multi-Frequency Signal Ratio (MFSR) of the received signal power between the high (60 MHz) and low (25 MHz) frequency ranges of a novel wideband high-frequency coronary catheter.

3.2 Materials and Methodology

An experimental system, referred to as a *phantom*, was designed to allow simulated arterial ultrasound images to be collected and measurements to be made. Phantoms have been used in previous research to help interpret clinical scanning, validate measurements used in clinical practice and clinical research, and help characterize imaging systems in the development of new ultrasound techniques. The ultrasound

measurements taken using phantoms should be similar to scanning in patients. Imaging and measurement *in vivo* are critically dependent on the physical properties of the different tissues through which the ultrasound beam passes. Thus, it is critical that the relevant physical properties of the phantom be similar to human tissues.

For this study, a flow phantom was designed to mimic the flow of blood through a coronary vessel of 4mm in diameter under steady flow conditions only. Due to the complexity and numerous effects associated with non-steady flow conditions, it was determined that a steady flow be used in this experiment as the main goal is to provide feasibility of a signal processing technique.

3.2.1 Flow Phantom Setup

Figure 12 shows a blood flow diagram of the experimental setup used for the in-vitro study. The setup consists of a mechanical pump (Masterflex, Barrington, IL; Model No. 7520-40) to circulate the media throughout the model at a pump speed of 6 – 600 rpm. The system flow rate is monitored using a flow meter (Accucal®, Barnant Company; Model GF-6540-1230) that comes with a flow rate analysis software (Barnant Company; Model GF-4000) to correlate the flow meter scale reading (0-100) to an actual rate that depends on flow factors such as media density, viscosity, and temperature. Due to material and monetary constraints of this study a standard vascular phantom (ATS Laboratories, Bridgeport, CT; Model 524) was used to mimic coronary arterial tissue. The phantom consists of 4 lumen channels, 14 cm in length, with diameters of 2, 4, 6, and 8 mm. For the purpose of this study, the center region of the 4 mm diameter channel was used because the 2mm channel does not provide a large enough imaging field for data

collection, while the 6 and 8 mm channels are not likely to be seen in clinical practice – most coronary arteries range between 2 – 4 mm [60]. The phantom is composed of a urethane rubber with a speed of sound equal to 1460 m/s with an attenuation coefficient of 0.5 dB/cm/MHz. Geometrical considerations of the vascular phantom will be discussed in the next section. This phantom was chosen for this study because it produced characteristics that closely reflect what would be seen in clinical practice.

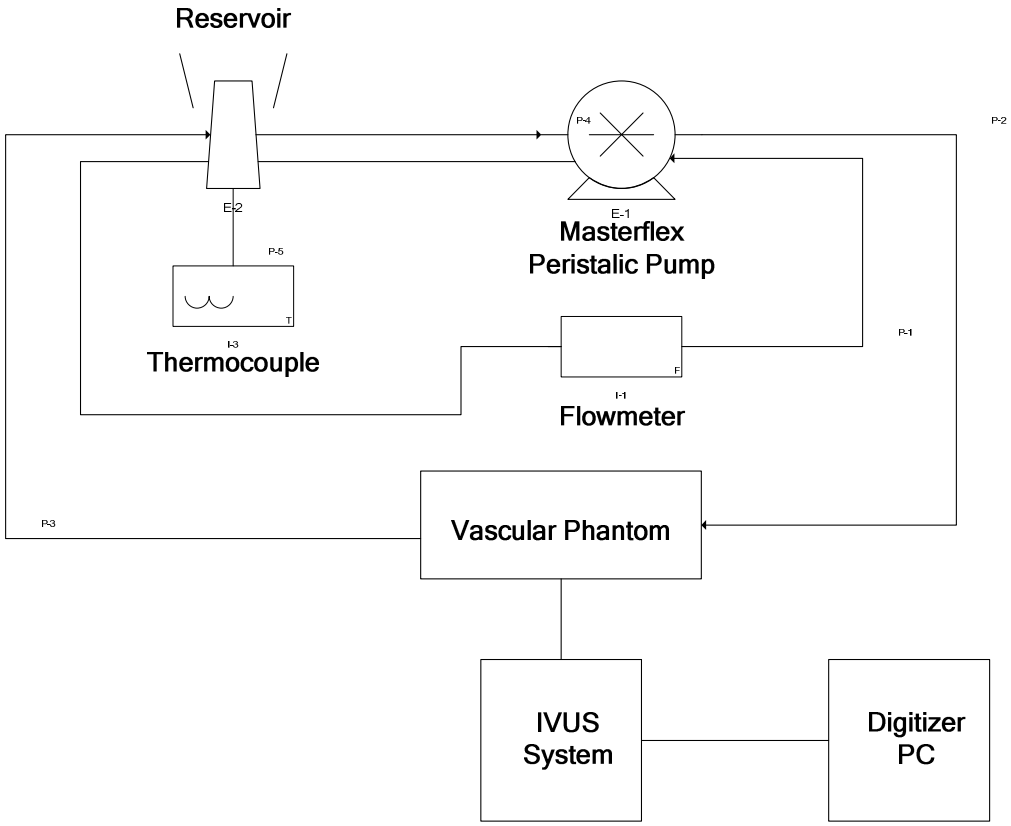

Figure 12: Blood Flow Model Diagram

The actual setup is shown in **Figure 13** and consists of two loops (see **Figure 12**): the main loop is used for porcine blood flow and imaging while the secondary loop is used to determine the flow velocity using Blood-Mimicking Fluid (BMF). Two loops

were used in this setup mainly because the color of the porcine blood would make it difficult to read the flowmeter scale, so the BMF which has more of a transparent characteristic was pumped in the secondary loop.

The physical and acoustic properties of the BMF and human blood are compared in **Table 1** below. The blood mimicking fluid consists of an Orgasol™ 5 µm nylon scattering particle and is described in further detail in previous work [91]. A sample of porcine whole blood was collected, with EDTA solution (25% HMT) as an anticoagulant, from a local animal laboratory. Within the main loop, the mechanical pump was used to control the flow speed within the system. Downstream from the pump is the vascular phantom that consists of a 4mm diameter channel made of rubber urethane. Due to its acoustic properties, the vascular phantom is used to mimic a coronary vessel in the heart and it is the location of the imaging window – the point at which the imaging catheter rests and performs imaging. A hot plate is used to control the temperature of the porcine blood at 37.5° C ± 0.5 by providing a feedback loop to the temperature controller. At the same time, a magnetic stir bar is placed within the blood reservoir to prevent aggregation within the flow loop. This temperature was chosen as it closely mimics the core temperature of human blood. As shown in **Figure 13,** the Masterflex tubes connecting each component together were tightly wrapped in aluminum foil. The purpose of this was to minimize the thermal loss experienced by the blood as it traveled through the system. At the same time, a heater pump (outside of view) was used to pump heated water over the top of the vascular phantom where most of the heat seemed to escape. A simple experiment showed that this method reduced the thermal effects experienced on the system by approximately 2° C.

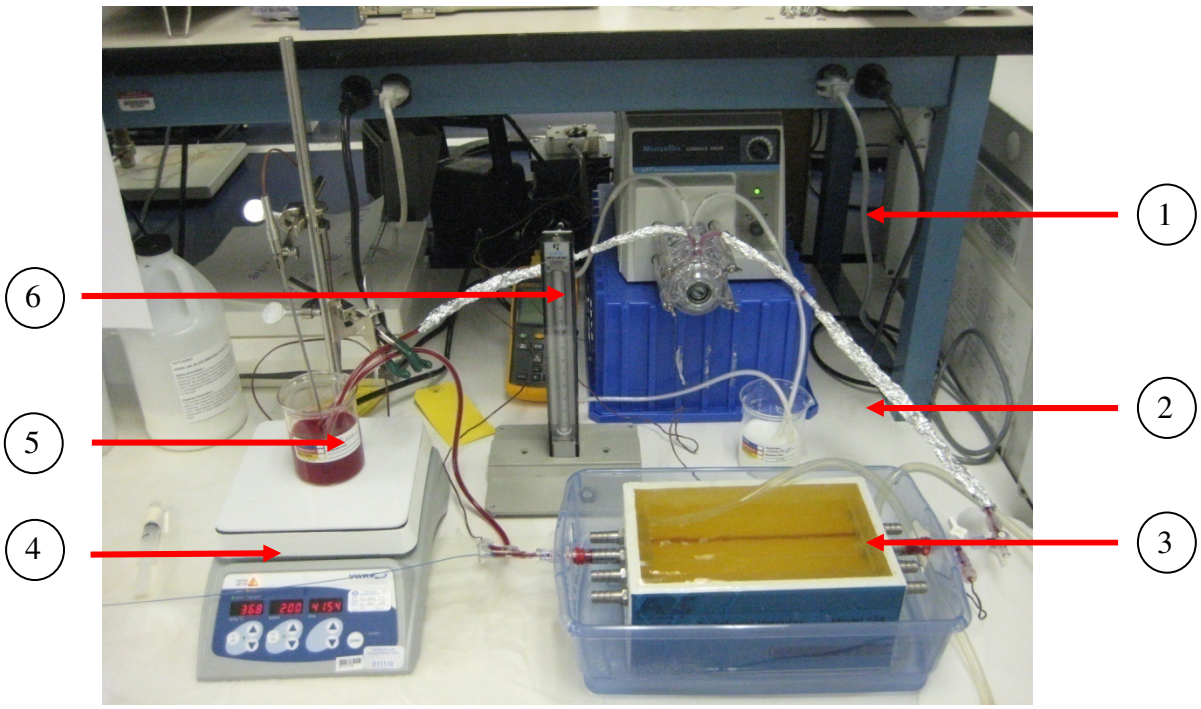

Figure 13: Blood flow model setup. (1) Masterflex mechanical pump, (2) Blood-Mimicking Fluid, (3) Vascular Phantom, (4) Hot Plate, (5) Porcine blood reservoir, (6) Flowmeter. Not shown is a water pump that was used to pump warm water over the surface of the vascular phantom (3) in order to optimize thermal losses within the system, keeping the blood at a nominal temperature of 37.5° C.

Table 1: Physical and acoustic properties of blood-mimicking fluid compared to whole human blood.

Properties	Human Blood (37°C)	Blood-Mimicking Fluid
Scatterer	Red blood cells	Orgasol™ (nylon particles)
Scatterer size (µm)	7	5
Hematocrit (% volume)	45	< 5
Density (kg m^{-3})	1053	1037 ± 2
Viscosity (mPa s)	3	4.1 ± 0.1
Velocity (m s^{-1})	1583	1548 ± 5
Attenuation (dB/cm/MHz)	0.15	0.05 ± 0.01

3.2.2 Vascular Phantom

For this study, the imaging catheter was inserted into the 4mm diameter channel of the vascular phantom, approximately 7 cm into the lumen to ensure the entrance length of the fluid media had reached a full velocity profile. In long and straight pipes, we know the flow is axial and axisymmetric [92], and given that the channel is rigid, the velocity profile can be described analytically. In a straight channel, the velocity profile will change with time and distance from the entrance of the tube, remaining unchanged beyond a certain distance called the *inlet length*. For steady flow, the velocity profile beyond the inlet length is parabolic (see **Figure 14**). Generally, the insonation region is the region beyond the inlet length where the velocity profiles are stable with distance (i.e. where imaging occurs). For this study, the insonation region was within the 7 cm inlet length designed for the flow phantom. The formula for the inlet length is given by [92;93]:

$$L = 0.04 d R_e \qquad 11$$

where L is the entrance length, d is the diameter of the tube. In order to maintain laminar flow, the Reynold's number must be less than the critical value of 2000 as given by [92]:

$$R_e = \frac{V d \rho}{\mu} \qquad 12$$

where V is mean velocity, ρ is density, μ is dynamic viscosity, and Re is the Reynolds number. Knowing the mean velocity and diameter of the vessel, we can determine the Reynold's number, which is an indication of whether or not the velocity profile will be

stable. Given the physical properties of blood shown in **Table 1** previously, the Reynold's number calculated from equation 12, and outlined in

Table 2, is valid for steady flow given the range of mean flow velocities. Thus, with a max Re of 421, a minimum entrance length of 6.73 cm is needed for a time-varying velocity profile to become fully developed; for this study, the designed inlet length satisfies the theoretical inlet length.

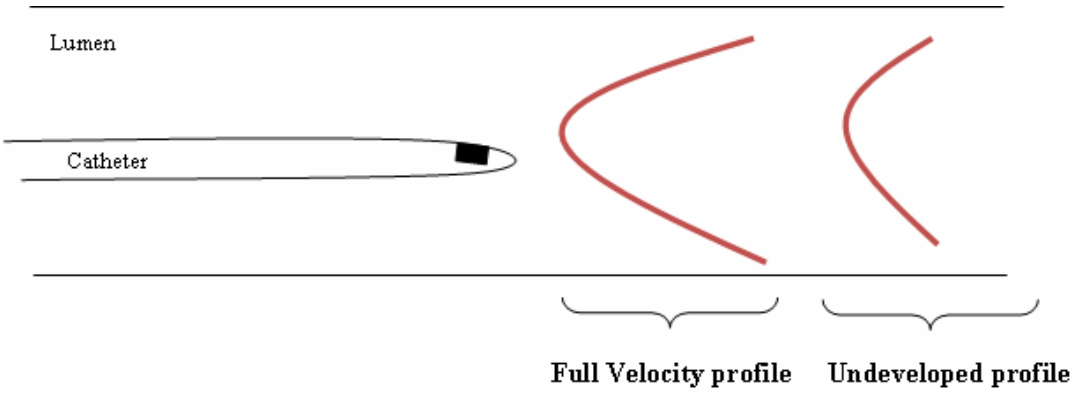

Figure 14: Velocity Profile Diagram

Table 2: Reynold's number and stability at varying mean flow velocities.

Mean Flow Velocity (cm/s)	Reynolds Number (R_e)	Flow Stability
0	0	Laminar
5	70	Laminar
10	140	Laminar
15	210	Laminar

20	280	Laminar
25	351	Laminar
30	421	Laminar

3.2.3 Intravascular Ultrasound Imaging System

The iLab™ ultrasound imaging system was provided by Boston Scientific (Natick, MA, USA). The imaging system consists of two PC's and a motor drive unit. The acquisition PC is where the raw RF data is filtered, enveloped, and other digital signal processing methods are performed. The data was then transferred from the acquisition PC to an imaging PC, where the data is scan converted into a two dimensional grey-scale image. The motor drive unit (MDU) is another peripheral component to the iLab™ system and is the interface between the coronary imaging catheter and the iLab™ system. The coronary catheter had a center frequency of 40MHz and a bandwidth of 80%. The MDU drives the cable shaft at 1800 rpm and sends the transmission pulse to the transducer element that is housed at the distal tip of the catheter.

3.2.4 Coronary Catheter

A coronary catheter with a novel transducer was used for this study in order to take complete advantage of capturing the high and low frequencies. Typical coronary catheter transducers have a center frequency of 40 MHz with a 40% bandwidth (BW). In other words, most of the used signal power, i.e. – 6dB fractional BW, from the transducer will range from 26 to 56 MHz. Using a catheter with such low BW will not allow us to capture data that can be differentiated between the high and low frequency (as will be explained later) – in this case, the high frequency would be 26 MHz and the low would be 56 MHz.

A novel transducer developed by Jian Yuan et al. [94] provided 80% BW. **Figure 15** provides a graphical representation of the difference in frequency response for a typical 40% BW coronary catheter and a high BW catheter at 80% BW, both with the same center frequency. **Figure 16** now compares the frequency responses of the coronary transducers to a typical frequency response of blood and tissue. We can see that for a typical 40% BW catheter, the responses for blood and tissue are outside the boundaries as to where the catheter can perform. On the other hand, the blood and tissue responses seem to be enveloped by the frequency response of the 80% BW catheter.

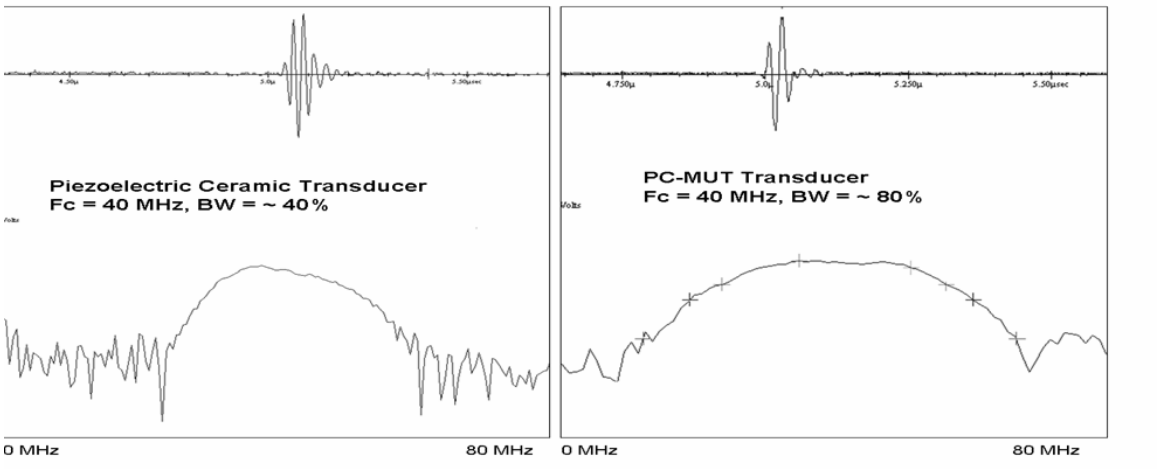

Figure 15: Frequency Response of High Bandwidth Transducer: The graph on the left represents the frequency response for a typical 40 MHz 10% BW coronary catheter transducer. The graph on the right depicts the frequency response of a higher bandwidth transducer, approximately 80%. [Image provided by Boston Scientific]

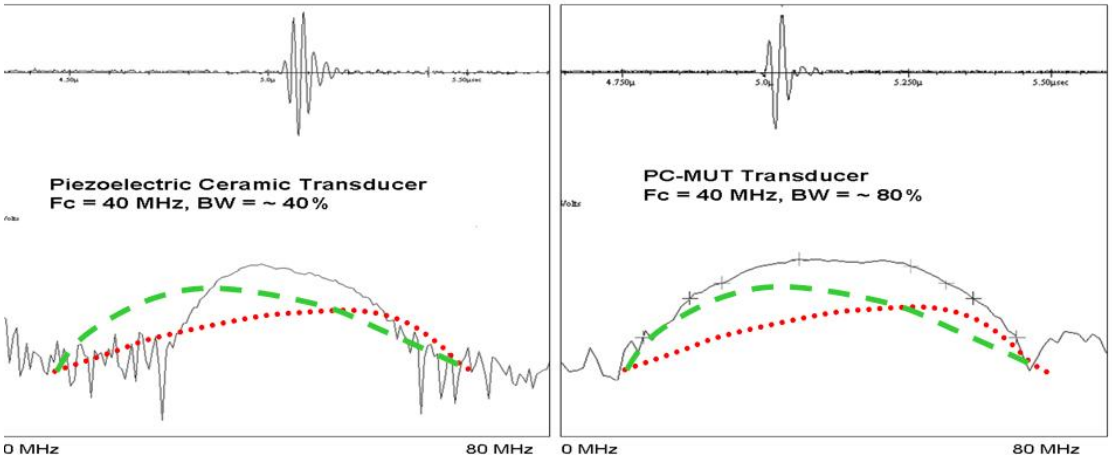

Figure 16 Blood and Tissue Frequency Response: The red dotted line portrays a typical blood frequency response while the green dashed line indicates the frequency response for normal arterial tissue. These tissues are prominent at different frequencies, which is the foundation of this study.

This novel, high bandwidth, coronary catheter transducer enables this study to collect data at a low and high enough frequency to enable us to study the potential differences of backscatter response at those frequencies to determine frequency dependency.

3.2.5 Data Acquisition and Analysis

Two 12-bit, Agilent Technologies PCI analog-to-digital converter boards (Acqiris DP310, Monroe, NY), along with Matlab® software, were used to collect original RF data for post-processing analysis. The RF data was sampled at a 400 MHz sampling frequency and divided into a 2048x256 matrix, where one matrix represents a single IVUS frame.

The number of frames collected was not a factor for data analyses since imaging was performed at a stationary position where all frames essentially represent the same RF data. In order to determine the power ratio at each flow velocity, a fourth order Butterworth band-pass digital filter was used to suppress everything but the high-frequency (60MHz 30% BW) and low-frequency (25MHz 80% BW) data from the original RF data set. The filtered data was then squared and averaged to determine the mean power signal.

A region of interest (ROI) was selected within two to three millimeters from the center of the lumen to represent blood data within the vessel under study (see ROI#1 in **Figure 17**). ROI #2 represents data that reflects a region of the vessel comprised of tissue only. Each ROI contained 300 total samples of data, where 10 vectors of 30 samples per vector were collected.

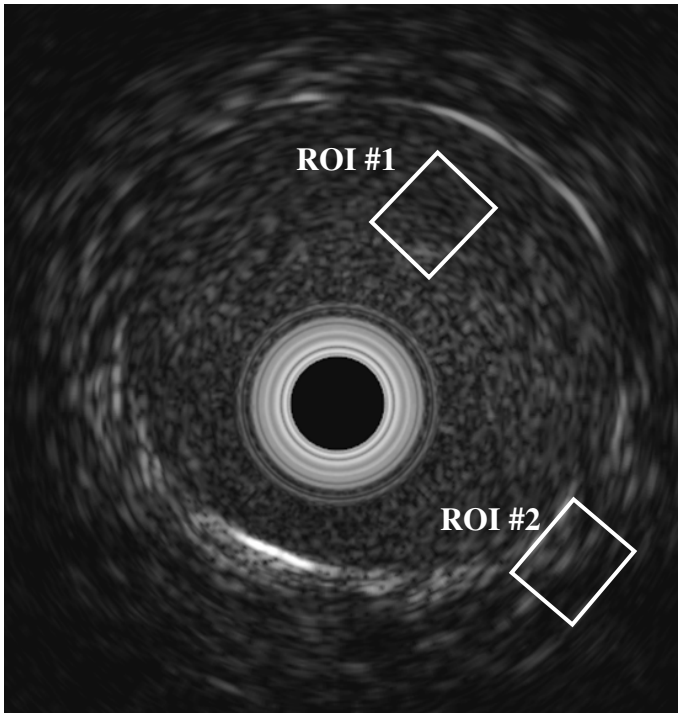

Figure 17: Region of Interest (ROI): ROI#1 represents blood data collected within the vessel lumen. ROI#2 represents tissue data collected of the same vessel. Each ROI contains 10 vectors or columns of data, and each vector comprises of 30 samples for a total of 300 samples per ROI.

High-frequency data (60MHz 30% BW) and low-frequency data (25MHz 80% BW) were collected for each ROI. Each vector was averaged and then the average of all the vectors within a ROI was calculated. For high-frequency data A_{60} represents the average power for a particular ROI. A_{25} represents the low-frequency average power for a particular ROI. Thus, in order to determine the Multi-Frequency Signal Ratio, or MFSR, the following equation was derived:

$$MFSR = \frac{A_{60}}{A_{25}} \qquad 13$$

The MFSR, where the high-frequency data (average power signal) is divided by the low-frequency average power signal, was calculated for each ROI.

The MFSR is what tells us if there is a correlation between the high-frequency (HF) filtered data and the low-frequency (LF) filtered data. The greater this ratio, the less correlation there is, meaning the HF and LF data do not match. In other words, the greater the MFSR value, the greater the sample is frequency dependent. If the HF and LF data do match, we would see a low MFSR value, indicating that biological tissue is not affected by frequency (frequency independent) and will be difficult to differentiate biological tissues using different frequencies. **Figure 18** provides an overview of the post-analysis process.

Before continuing on, it is important to note why the 60 MHz and 25 MHz frequencies were used for this experiment. As mentioned previously, the center frequency of the imaging catheter was 40MHz, but the important part is its ability to transmit with 80% bandwidth. Essentially the catheter can transmit signals from 8MHz to 72 MHz. Since the transmitted power is max at the center frequency (40MHz) and derates at all other frequencies, we wanted to capture the highest and lowest frequencies that can still transmit a lot of power. At -3dB, 50% of the max power is being generated, so any frequencies within the -3dB range will suffice. The 25 and 60MHz frequencies lie within this range and provide a broad enough spectrum for testing the MFSR theory.

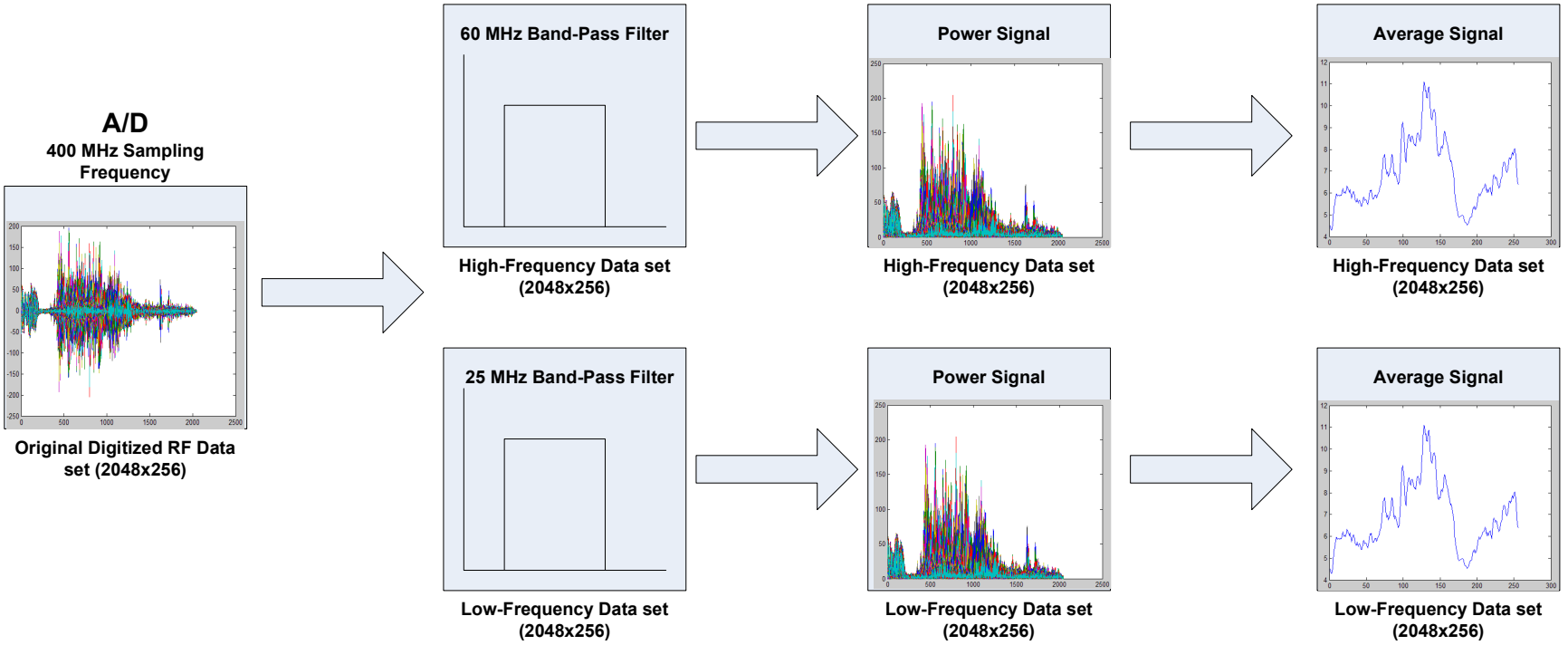

Figure 18: Multi-frequency post-processing analysis flowchart. The final step in this post-analysis process is to take the average of the averaged signal shown above, which is not shown. This final numerical value provides us with A60 and A25. Taking the ratio of A60 over A25, we can determine the MFSR and ultimately understand whether or not that particular sample is frequency dependent.

3.3 Results and Discussion

3.3.1 In-Vitro Study

The MFSR results for the porcine blood at various flow velocities and for the tissue mimicking wall are summarized in **Table 3**. Examining the data for mean flow velocity for blood gave us an MFSR of 2.77 (43.73 / 15.76 = 2.77), but the MFSR for tissue is 0.28 (17.44 / 61.18 = 0.28). As mentioned previously, the higher the MFSR, the more dependent the data is on frequency. The MFSR values of blood regions are consistently higher than those measured from the wall, where blood has an average MFSR value 8x greater than that of tissue. What this means is that the intensity of the backscattering level for blood is much greater than tissue at higher frequencies, making it easy for an algorithm to detect which RF signals are blood and tissue. One interesting observation was the MFSR value was higher at the low flow velocities then at all other velocities, which may provide a unique advantage in detecting blood speckle under stagnant flow. The underlying physics of this phenomenon still need to be understood but can mostly be attributed to the rouleaux phenomenon – as described by previous studies cited in this chapter. This rouleaux phenomenon causes the blood cells to clump or stick together, essentially becoming denser and more echogenetic, or better said, the blood cells backscatter intensity will increase because the cell size increases. This method is advantageous over current blood detection methods used clinically in that those methods use a time-based correlation technique which does not work well in low flow environments as these methods expect blood to be rapidly changing continuously but is not always be the case. A more visual representation of **Table 3** can be found in **Figure**

19 – the MFSR values are plotted against velocity, all other data from Table 3 was omitted from this plot.

The results in **Table 3** give us insight into the ability to use the MFSR technique to clearly detect blood flow within a vessel and better delineate the lumen boundary between blood and tissue. As mentioned previously, this is advantageous because it enables physicians to better determine the lumen diameter of a diseased vessel and provide the right therapy.

Table 3: MFSR results for whole porcine blood (37.5°C) and a tissue-mimicking media

	Porcine Blood (25% Hematocrit)			**Tissue-Mimicking Wall (TMW)**		
Mean Flow Velocity (cm/s)	HF Signal Power	LF Signal Power	MFSR	HF Signal Power	LF Signal Power	MFSR
0	71.12	27.36	2.59	16.25	54.99	0.29
5	43.73	15.76	2.77	17.44	61.18	0.28
10	35.13	14.75	2.38	17.75	57.07	0.31
15	33.54	14.75	2.27	17.54	63.39	0.27
20	33.40	14.9	2.23	15.61	48.48	0.32
25	34.12	15.29	2.23	19.09	65.40	0.29
30	37.04	15.91	2.32	18.52	67.05	0.27

A quantitative analysis is shown in **Figure 20** as it provides a plot of the backscatter intensity (amplitude) in the blood regions at varying flow rates. We can see that MFSR for blood is greater at all flow velocities at higher frequencies (60 MHz) compared to the lower frequency (25 MHz). It is important to note that there is a jump in intensity with blood at the stagnant flow region (0 cm/s) and can be associated with the lack of movement in the vessel and increased cell size of blood (due to rouleaux). When

the vessel is not moving the noise in the system is minimized and it will be easier for the receiver to pick up all signals from the cells (due to less interference), thus increasing the intensity of the received signal. Although blood has increased amplitudes at stagnant flow, we can attribute some of it to a stable, non-moving system rather than attributing it to this MFSR technique.

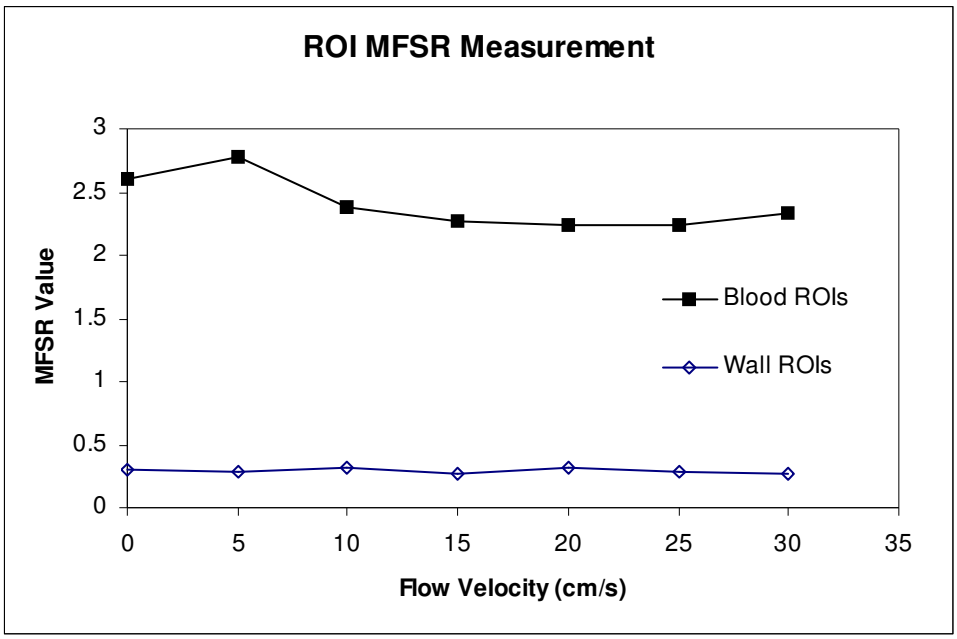

Figure 19: Mean Multi-Frequency Signal Ratio values measured in the blood-filled and wall regions with varying flow rates. The values are consistently higher for the blood than the tissue of the entire range of the flow rates.

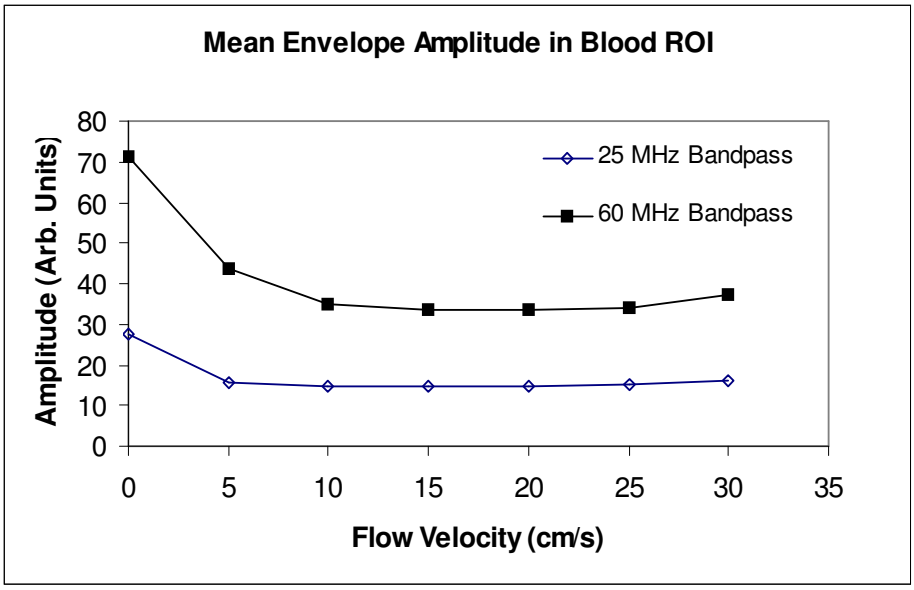

Figure 20: Mean signal amplitudes with the 60 and 25 MHz band-pass filters measured in the blood-filled ROI.

Appendix A provides an understanding of IVUS images and portrays the lumen enhancement technique implemented using the data captured from this in vitro study. The images portray the blood and tissue becoming more apparent at the frequencies used for this study and indicates visually that this method can be verified qualitatively. The left image is the conventional 40 MHz (40% bandwidth) IVUS image within the blood flow phantom as used in the study. The 40 MHz image shown has not been post-processed in any way. The middle and right images have been multi-frequency processed as described in the Data Acquisition section above.

According to the studies presented earlier on the properties of blood and tissue, we would expect to see the tissue to be the most prominent scattering element when filtered at lower frequencies, and blood to be the most prominent scatterer at higher frequencies. The 25 MHz image in the middle clearly highlights the tissue mimicking media within the vascular phantom; the porcine blood is indistinguishable. However, the

60 MHz filtered image clearly distinguished the porcine blood in the image, and this time the tissue has been attenuated – suggesting tissue is frequency dependent at lower frequencies and blood is frequency dependent at higher frequencies. This comparison qualitatively indicates that there is a clear distinction between the blood and tissue when using the multi-frequency processing technique suggested in this paper.

3.3.1 In-Vivo Study

Figure 21: In vivo coronary image showing visual enhancement of a thrombus (Arrow). **A) 40-MHz high resolution IVUS image. B) MFSR image obtained but the multi-frequency processing. C) Color-coded blood speckles to enhance the arterial lumen. The thrombus is difficult to recognize due to its echo intensities similar to blood, particularly, on the still frame.Figure 21** shows the lumen enhancement obtained from an *in vivo* animal study. This example demonstrates the ability of this method to produce a clean delineation between the arterial wall and blood.

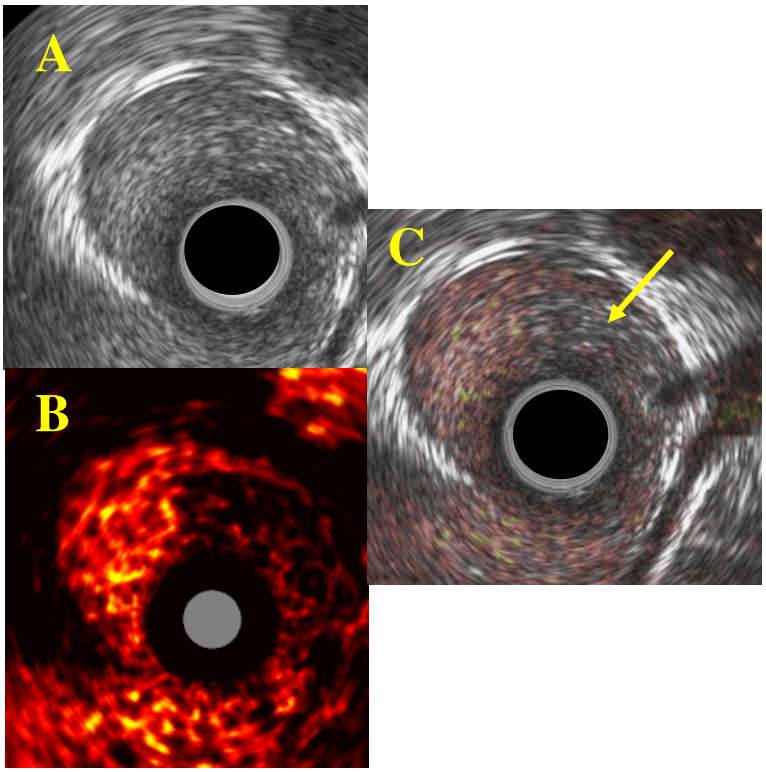

Figure 21: In vivo coronary image showing visual enhancement of a thrombus (Arrow). A) 40-MHz high resolution IVUS image. B) MFSR image obtained but the multi-frequency processing. C) Color-coded blood speckles to enhance the arterial lumen. The thrombus is difficult to recognize due to its echo intensities similar to blood, particularly, on the still frame.

This study helps qualitatively validate this multi-frequency technique. Furthermore, this study helps demonstrate the MFSR technique to produce a clear delineation of the thrombus, which is otherwise difficult to recognize because it was surrounded by blood speckles having similar intensities.

3.4 Conclusion

Strong scattering from blood due to the use of high ultrasonic frequencies has been a constant challenge for improving IVUS image quality. Most of the previously reported IVUS lumen enhancement techniques have taken advantage of the fast and random frame-to-frame movement of blood speckles in contrast to the slow and

consistent motion from the tissue [95;96]. This motion contrast is also the most important visual cue to physicians unless saline is injected to flush out the lumen. One common drawback of a motion-based method is its inability to detect blood speckle effectively at low flow velocities, which is often seen in severe flow-limiting lesions. Other clinical applications, such as identifying small dissections, thrombi, or mild stent malappositions may also require dealing with a low flow condition where blood speckle does not always present a clear motion contrast. The unique advantage of the multi-frequency approach is that it does not rely on blood-tissue motion differences and, as demonstrated by the results in Error! Reference source not found., this method was able to enhance the lumen even when there was no blood flow (stagnant flow) in the phantom. Furthermore, this method does not require processing image data from multiple vectors or multiple frames, allowing it to be free of motion-induced smearing artifacts that may hinder a motion-based method.

One limitation of this method is the inhomogeneous image intensity due to the nature of ultrasound imaging. The MFSR value may vary significantly due to intensity variation of the speckle. Spatial averaging may be necessary to reduce this variation but it may also limit the resolution of the MFSR image.

The multi-frequency processing technique verified that the backscatter power from blood is proportional to frequency as reported by other groups, where tissue does not seem to have the same response. In fact, it was found that at 60 MHz the tissue had been greatly attenuated, whereas the blood scatter power increased. At low shear rates ($\leq$5 cm/s), the MFSR for blood was approximately 9x greater than the ratio for tissue. Furthermore, at high shear rates ($\geq$20 cm/s), the MFSR for blood was an average of 7x

greater than the MFSR for tissue. This effect provides a feasible method for lumen enhancement, allowing physicians to better assess the blood-wall boundary and determine the severity of atherosclerotic region. Although tissue-mimicking media is designed to model in vivo tissue, there are a lot of dynamics that affect the attenuation of ultrasound and it would be beneficial to collect RF data from in vivo studies to better determine the accuracy of the multi-frequency technique described in this paper.

The experimental technique described in this paper has the potential of being applied to flow velocity measurements. It was found that the MFSR decreased with velocity; however, further research needs to be performed on velocities greater than 30 cm/s.

As mentioned in previous sections, blood backscatter relies on many factors other than the flow velocity. It is recommended that further research be developed to understand whether or not the method proposed in this report would be clinically acceptable. Currently, detecting thrombus in IVUS is difficult as it has similar acoustic properties as an atheroma with high lipid content [97]. The MFSR technique, during un-documented tests, indicated the detection of thrombus, which is a serious risk factor when diagnosing a patient. Further studies to ensure validity of these findings should be considered.

As center frequencies increase to improve image resolution, more work on multi-frequency processing at higher frequencies needs to be addressed since blood scattering may become so intense that it will then interfere with disease identification.

Furthermore, flow velocity became apparent when analyzing the results during the study. Further work involving the MFSR technique to help estimate flow velocities

would significantly aid the characterization of disease within a vessel. If it was estimated that a low flow state was detected, then one might assume that the severity of the disease is significant and would require further investigation of the vessel.

Appendix A

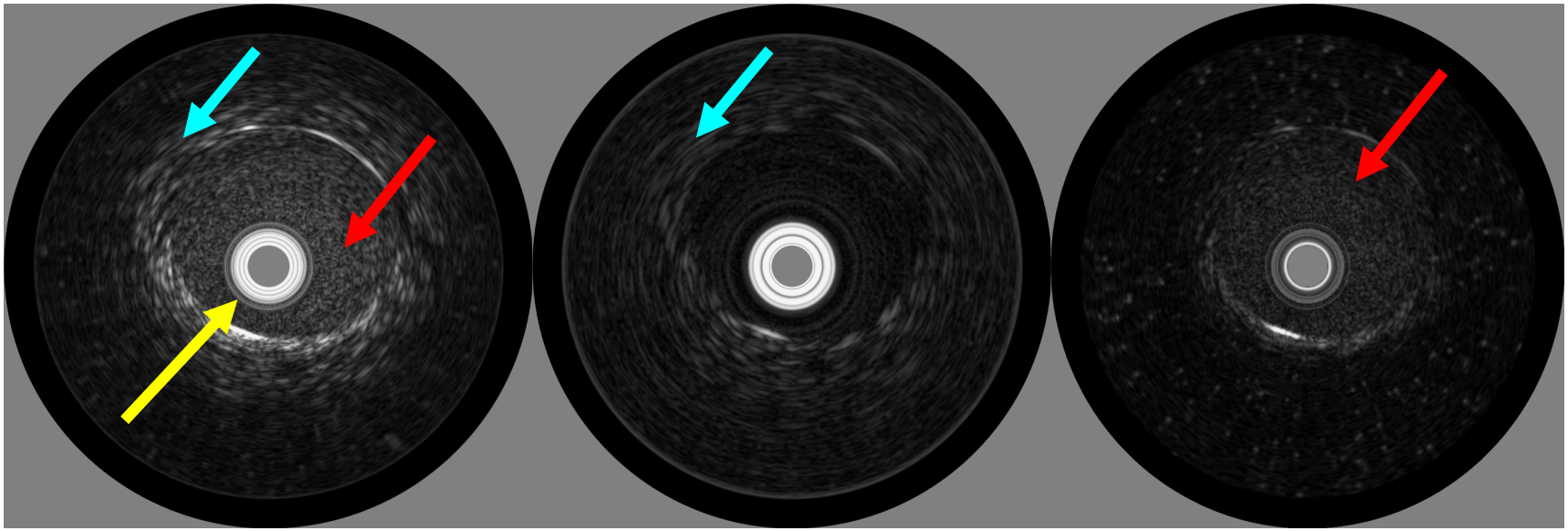

Figure 22: Enhanced Image Analysis: Standard 40 MHz IVUS image (Left). 25 MHz filtered image (Middle). 60 MHz filtered image (Right). This comparison clearly distinguishes the porcine blood at high frequencies and tissue at lower frequencies.

The IVUS images above can be hard to understand if you are not familiar with IVUS technology. The image on the far left has not been post-processed in any way. Looking at this image you will notice in the very center a gray circle with bright rings around it (see Yellow arrow). This whole area is due to the catheter sheath that covers the transducer within the catheter. Essentially, this gray circle and bright concentric rings surrounding it can be ignored as they are not important when looking at IVUS images. When looking

at the rest of the image you will notice regions that are brighter than others (see Blue arrow). These regions correspond to normal tissue within the coronary arteries. Normal tissue is characterized by having a good scattering effect and long rod-like shapes. The red arrow indicates the region in which blood flows. The backscatter level here is typically lower than tissue and its texture much more fine than normal tissue – it can be better described as looking at static while watching TV.

The middle image is a representation of the image on the far left, except this image has been post-processed and filtered at 25MHz. This means only data within 25MHz will be present in the image. We can see from this image that tissue is more prominent and has a higher backscatter response at lower frequencies (see the Blue arrow), whereas blood is barely visible in this image. The far right image has been processed at 60MHz. Here it is evident that the blood is the most prominent scattering element in the image (see Red arrow) – it is also apparent that the tissue has been filtered. The difference between these two images is the essence of how the MFSR value is calculated and what enables the enhancement of the lumen boundary.

Bibliography

[1] W. Rosamond, K. Flegal, G. Friday, K. Furie, A. Go, K. Greenlund, N. Haase, M. Ho, V. Howard, B. Kissela, S. Kittner, D. Lloyd-Jones, M. McDermott, J. Meigs, C. Moy, G. Nichol, C. J. O'Donnell, V. Roger, J. Rumsfeld, P. Sorlie, J. Steinberger, T. Thom, S. Wasserthiel-Smoller, Y. Hong, and for the American Heart Association Statistics Committee and Stroke Statistics Subcommittee, "Heart Disease and Stroke Statistics--2007 Update: A Report From the American Heart Association Statistics Committee and Stroke Statistics Subcommittee," *Circulation*, vol. 115, no. 5, pp. e69-171, Feb.2007.

[2] S. E. Nissen, J. C. Gurley, C. L. Grines, D. C. Booth, R. McClure, M. Berk, C. Fischer, and A. N. DeMaria, "Intravascular ultrasound assessment of lumen size and wall morphology in normal subjects and patients with coronary artery disease," *Circulation*, vol. 84, no. 3, pp. 1087-1099, Sept.1991.

[3] C. Berry, P. L. L'Allier, J. Gregoire, J. Lesperance, S. Levesque, R. Ibrahim, and J. C. Tardif, "Comparison of Intravascular Ultrasound and Quantitative Coronary Angiography for the Assessment of Coronary Artery Disease Progression," *Circulation*, vol. 115, no. 14, pp. 1851-1857, Apr.2007.

[4] Guyton A.C.and Hall J.E., *Human Physiology and mechanics of disease*, 6 ed. Philadelphia: W.B Saunders Company, 1997.

[5] Marieb E.N.., *Anatomy & Physiology*. San Francisco: Benjamin Cummings, 2004.

[6] Libby P, "Inflammation in atherosclerosis," *Nature*, vol. 420(6917), pp. 868-874, 2002.

[7] W. E. Z. C. S. R. K. Glagov S and s GJ, "Compentsatory enlargement o fhuman athersclerotic coronary arteries," *New Engalnd Journal of Medicine*, no. 316, pp. 1371-1375, 1987.

[8] G. Liepa, "Cardiovascular Disease: Diet, Nutrition, and Emerging Risk Factors: The Report of a British Nutrition Foundation Task Force," *Nutr Clin Pract*, vol. 21, no. 3, p. 320, June2006.

[9] P. A. K. D. M. K. a. M. J. D. A.C.Thomas, "Community study of the causes of "natural" sudden death.," *British Medical Journal*, vol. 297, no. 6661, pp. 1453-1456, Dec.1988.

[10] E. Escolar, G. Weigold, A. Fuisz, and N. J. Weissman, "New imaging techniques for diagnosing coronary artery disease," *CMAJ*, vol. 174, no. 4, pp. 487-495, Feb.2006.

[11] W.FORSSMAN, "**Die Sondierung dec rechten Herzen**,", 8 ed 1929, pp. 2085-2087.

[12] E. K. S. F.M.Sones, "Acquired heart disease: symposium on present and future cineangiocardiography," *J Am Coll Cardiol*, vol. 3, p. 710, 1959.

[13] Sones F.M. and Shirley E.K., "Cine coronary arteriography," *Mod Concepts Cardiovasc Dis*, vol. 31, p. 735, 1962.

[14] M.P.Judkins, "Selective Coronary Angiography: A percutraneous transfemoral technic," *Radiology*, vol. 89, pp. 815-824, 1967.

[15] "American Heart Association Heart and stroke facts 2003 Statistical supplement," *American Heart Association*, pp. 1-46, 2003.

[16] Baim DS, *Cardiac Catheterization, Angiography, and Intervention*, 7 ed Lippincott Williams & Wilkins, 2005.

[17] P. J. Scanlon, D. P. Faxon, A. M. Audet, B. Carabello, G. J. Dehmer, K. A. Eagle, R. D. Legako, D. F. Leon, J. A. Murray, S. E. Nissen, C. J. Pepine, R. M. Watson, J. L. Ritchie, R. J. Gibbons, M. D. Cheitlin, K. A. Eagle, T. J. Gardner, A. Garson, Jr., R. O. Russell, Jr., T. J. Ryan, and S. C. Smith, Jr., "ACC/AHA Guidelines for Coronary Angiography: Executive Summary and Recommendations : A Report of the American College of Cardiology/American Heart Association Task Force on Practice Guidelines (Committee on Coronary Angiography) Developed in collaboration with the Society for Cardiac Angiography and Interventions," *Circulation*, vol. 99, no. 17, pp. 2345-2357, May1999.

[18] V. R. F. L. S. HC. Hanley PC, "Indications for coronary angiography: changes in laboratory practice over a decade.," *Mayo Clinic Proceedings*, vol. 61, pp. 248-253, 1986.

[19] v. d. Z. P. K. G. e. al. Reiber JH, "Accuracy and precision of quantitative digital coronary arteriography: observer-, short-, and medium-term variabilities.," *Catheterization and Cardiovascular Diagnosis*, vol. 28, pp. 187-198, 1993.

[20] "1992 Hospital charges for two major surgical procedures for cardiovascular diseases. Part II: Cardiac Catheterization.,", 75 ed 1994, pp. 21-28.

[21] Agency for Healthcare Research and Quality, "Healthcare Cost and Utilization Project," Washington, DC: 2000.

[22] C. M. GRONDIN, I. H. O. R. DYRDA, A. N. D. R. PASTERNAC, L. U. C. I. CAMPEAU, M. G. BOURASSA, and J. A. C. Q. LESPERANCE, "Discrepancies Between Cineangiographic and Postmortem Findings in Patients with Coronary Artery Disease and Recent Myocardial Revascularization," *Circulation*, vol. 49, no. 4, pp. 703-708, Apr.1974.

[23] A. DeFranco, "Understanding the pathophysiology of the arterial wall: which method should we choose? Intra-vascular ultrasound," *Eur Heart J Suppl*, vol. 4, no. suppl_F, p. F29-F40, Sept.2002.

[24] C. PJ. Blankenhorn DH, "The accuracy of arteriography and ultrasound imaging for atherosclerosis measurement: a review.," *Archives of Pathology and Laboratory Medicine*, no. 106, pp. 483-489, 1982.

[25] J. M. Isner, J. Kishel, K. M. Kent, J. A. Ronan, Jr., A. M. Ross, and W. C. Roberts, "Accuracy of angiographic determination of left main coronary arterial narrowing. Angiographic--histologic correlative analysis in 28 patients," *Circulation*, vol. 63, no. 5, pp. 1056-1064, May1981.

[26] F. G. Goar, F. J. Pinto, E. L. Alderman, H. A. Valantine, J. S. Schroeder, S. Z. Gao, E. B. Stinson, and R. L. Popp, "Intracoronary ultrasound in cardiac transplant recipients. In vivo evidence of "angiographically silent" intimal thickening," *Circulation*, vol. 85, no. 3, pp. 979-987, Mar.1992.

[27] E. J. Gussenhoven, C. E. Essed, C. T. Lancee, F. Mastik, P. Frietman, F. C. van Egmond, J. Reiber, H. Bosch, H. van Urk, and J. Roelandt, "Arterial wall characteristics determined by intravascular ultrasound imaging: an in vitro study," *J Am Coll Cardiol*, vol. 14, no. 4, pp. 947-952, Oct.1989.

[28] J. M. Tobis, J. Mallery, D. Mahon, K. Lehmann, P. Zalesky, J. Griffith, J. Gessert, M. Moriuchi, M. McRae, and M. L. Dwyer, "Intravascular ultrasound imaging of human coronary arteries in vivo. Analysis of tissue characterizations with comparison to in vitro histological specimens," *Circulation*, vol. 83, no. 3, pp. 913-926, Mar.1991.

[29] W. C. Little, M. Constantinescu, R. J. Applegate, M. A. Kutcher, M. T. Burrows, F. R. Kahl, and W. P. Santamore, "Can coronary angiography predict the site of a subsequent myocardial infarction in patients with mild-to-moderate coronary artery disease?," *Circulation*, vol. 78, no. 5, pp. 1157-1166, Nov.1988.

[30] W. C. Roberts and A. A. Jones, "Quantification of coronary arterial narrowing at necropsy in acute transmural myocardial infarction. Analysis and comparison of findings in 27 patients and 22 controls," *Circulation*, vol. 61, no. 4, pp. 786-790, Apr.1980.

[31] A. Nair, B. D. Kuban, E. M. Tuzcu, P. Schoenhagen, S. E. Nissen, and D. G. Vince, "Coronary Plaque Classification With Intravascular Ultrasound Radiofrequency Data Analysis," *Circulation*, vol. 106, no. 17, pp. 2200-2206, Oct.2002.

[32] S. E. Nissen and P. Yock, "Intravascular Ultrasound : Novel Pathophysiological Insights and Current Clinical Applications," *Circulation*, vol. 103, no. 4, pp. 604-616, Jan.2001.

[33] S. E. Nissen and J. C. Gurley, "Application of intravascular ultrasound for detection and quantitation of coronary atherosclerosis," *The International Journal of Cardiac Imaging*, vol. 6, no. 3, pp. 165-177, Sept.1991.

[34] S. K. Mehta, J. R. McCrary, A. D. Frutkin, W. J. S. Dolla, and S. P. Marso, "Intravascular ultrasound radiofrequency analysis of coronary atherosclerosis: an emerging technology for the assessment of vulnerable plaque," *Eur Heart J*, vol. 28, no. 11, pp. 1283-1288, June2007.

[35] L. P. B. R. B. E. Zipes DP, *Braunwald's Heart Disease: A Textbook of Cardiovascular Medicine*, 7 ed. *St. Louis*: *W.B. Saunders*, 2005.

[36] J. Smith, T. E. Feldman, J. Hirshfeld, A. K. Jacobs, M. J. Kern, S. B. King III, D. A. Morrison, W. W. O'Neill, H. V. Schaff, P. L. Whitlow, D. O. Williams, E. M. Antman, J. Smith, C. D. Adams, J. L. Anderson, D. P. Faxon, V. Fuster, J. L. Halperin, L. F. Hiratzka, S. A. Hunt, A. K. Jacobs, R. Nishimura, J. P. Ornato, R. L. Page, and B. Riegel, "ACC/AHA/SCAI 2005 Guideline Update for Percutaneous Coronary Intervention: A Report of the American College of Cardiology/American Heart Association Task Force on Practice Guidelines (ACC/AHA/SCAI Writing Committee to Update the 2001 Guidelines for Percutaneous Coronary Intervention)," *J Am Coll Cardiol*, vol. 47, no. 1, p. e1-e121, Jan.2006.

[37] K. A. S. T. K. J. B. N. ten Hoff H, "Imaging artifacts in mechanically driven ultrasound catheters.," *Journal of Cardiac Imaging*, vol. 4, pp. 195-199, 1989.

[38] F. JT. Levin DC, "Significance of the angiographic morphology of localized coronary stenoses: histopathologic correlations.," *Circulation*, vol. 66, pp. 316-320, 1982.

[39] V. B. A. N. D. Bruce J.Kimura, "Value and limitations of intravascular ultrasound imaging in characterizing coronary atherosclerotic plaque," *American Heart Journal*, vol. 130, no. 2, pp. 386-396, 1995.

[40] B. J. Kimura, V. Bhargava, and A. N. DeMaria, "Value and limitations of intravascular ultrasound imaging in characterizing coronary atherosclerotic plaque," *American Heart Journal*, vol. 130, no. 2, pp. 386-396, Aug.1995.

[41] D. Huang, E. A. Swanson, C. P. Lin, J. S. Schuman, W. G. Stinson, W. Chang, M. R. Hee, T. Flotte, K. Gregory, C. A. Puliafito, and a. et, "Optical coherence tomography," *Science*, vol. 254, no. 5035, pp. 1178-1181, Nov.1991.

[42] O. C. Raffel, T. Akasaka, and I. K. Jang, "Cardiac optical coherence tomography," *Heart*, vol. 94, no. 9, pp. 1200-1210, Sept.2008.

[43] B. X. Chen, F. Y. Ma, W. Luo, J. H. Ruan, W. L. Xie, X. Z. Zhao, S. H. Sun, X. M. Guo, F. Wang, T. Tian, and X. W. Chu, "Neointimal coverage of bare-metal

and sirolimus-eluting stents evaluated with optical coherence tomography," *Heart*, vol. 94, no. 5, pp. 566-570, May2008.

[44] I. K. Jang, B. E. Bouma, D. H. Kang, S. J. Park, S. W. Park, K. B. Seung, K. B. Choi, M. Shishkov, K. Schlendorf, E. Pomerantsev, S. L. Houser, H. T. Aretz, and G. J. Tearney, "Visualization of coronary atherosclerotic plaques in patients using optical coherence tomography: comparison with intravascular ultrasound," *J Am Coll Cardiol*, vol. 39, no. 4, pp. 604-609, Feb.2002.

[45] H. K. Y. R. e. al. Kawase Y, "In vivo volumetric analysis of coronary stent using optical coherence tomography with a novel balloon occlusion-flushing catheter: A comparison with intravascular ultrasound.," *Ultrasound in Medicine and Biology*, no. 31, pp. 1343-1349, 2005.

[46] C. Curie.J.P., "Développement par pression de l'é'lectricite polaire dans les cristaux hémièdres à faces inclinées," *C. R. Acad. Sci (Paris)*, no. 91, p. 294, 1880.

[47] H. Feigenbaum, "Evolution of Echocardiography," *Circulation*, vol. 93, no. 7, pp. 1321-1327, Apr.1996.

[48] Sokolov S.Y., "Means for indicating flaws in materials," 1937.

[49] R. A. Meyer, "History of Ultrasound in Cardiology," *J Ultrasound Med*, vol. 23, no. 1, pp. 1-11, Jan.2004.

[50] P. G. Newman and G. S. Rozycki, "THE HISTORY OF ULTRASOUND," *Surgical Clinics of North America*, vol. 78, no. 2, pp. 179-195, Apr.1998.

[51] Acierno L.J. and Worrell L.T., "Inge Edler: Father of Echocardiography," *Clinical Cardiology*, vol. 25, pp. 197-199, 2002.

[52] C. H. R. J. Wild JJ, "Visualization of the excised human heart by means of reflected ultrasound or echocardiography," *American Heart Journal*, vol. 54, pp. 903-906, 1957.

[53] Kossoff G., "Diagnositc applications of ultrasound in cardiology," *Australas Radiology*, vol. 10, pp. 101-106, 1966.

[54] Carleton R.A., Sessions R.W., and Graettinger J.S., "Diameter of heart measured by intracavitary ultrasound," *Medical Research in Engineering*, no. May/June, pp. 28-32, 1969.

[55] Stegall H.F., Pratt J.R., and Moser P.F., "Carotic Mechanics in site," *Fed Proc*, vol. 28, p. 585, 1969.

[56] Wells P.N.T., "Development in medical ultrasonics," *World Medical Electronics*, vol. 66, no. 4, p. 272, 1966.

[57] Bom N, Lancee C.T., and van Egmond F.C., "An ultrasonic intracardiac scanner," *Ultrasonics*, vol. 10, pp. 72-76, 1973.

[58] Martin Dunitz, *Intravascular Ultrasound*. London: Martin Dunitz Limited, 1998.

[59] W.N.McDicken, *Diagnositc Ultrasonic Principles and Use of Instruments*. New York: Wiley Medical, 1981.

[60] K. K. Shung and G. A. Thieme, *Ultrasnoic Scattering in Biological Tissues*. Boca Raton, FL: CRC Press, 1993.

[61] Zagzebski J., *Essentials of Ultrasound Physics*. St Louis: Mosby Inc, 1996.

[62] Wells P.N.T, *Biomedical Ultrasonics*. New York: Academic Press, 1977.

[63] R. A. Meyer, "Intravascular ultrasound technological advances and clinical applications," *Progress in Pediatric Cardiology*, vol. 7, no. 3, pp. 141-153, June1997.

[64] F. S. Foster, H. Obara, T. Bloomfield, L. K. Ryan, and G. R. Lockwood, "Ultrasound backscatter from blood in the 30 to 70 MHz frequency range,", 3 ed 1994, pp. 1599-1602.

[65] Duck F.A, *Physical Properties of tissue*. London: Academic Press, 1990.

[66] S. H. O. H. N. S. T. M. Saijo Y, "Acoustic properties of atherosclerosis of human aorta obtained with high-frequency ultrasound.," *Ultrasound in Medicine & Biology*, no. 24, pp. 1061-1064, 1998.

[67] G. P. H. J. C. H. B. D. Rooney JA, "Velocity and attenuation of sound in arterial tissues," *J Am Coll Cardiol*, no. 71, pp. 462-466, 1982.

[68] S. W. J. S. Greenleaf JF Duck FA, "Ultrasonic data acquisition and processing system for atherosclerotic tissue characterisation," *Progress in Pediatric Cardiology*, no. 56, pp. 738-743, 1974.

[69] L. L. D. A. B. A. S. R. L. A. Picano E, "Fibrosis, lipids, and calcium in human atherosclerotic plaque—In vitro differentiation from normal aortic walls by ultrasonic-attenuation," *Circulation*, no. 56, pp. 556-562, 1985.

[70] G. R. Lockwood, L. K. Ryan, J. W. Hunt, and F. S. Foster, "Measurement of the ultrasonic properties of vascular tissues and blood from 35-65 MHz," *Ultrasound in Medicine & Biology*, vol. 17, no. 7, pp. 653-666, 1991.

[71] K. Hibi, A. Takagi, X. Zhang, T. J. Teo, H. N. Bonneau, P. G. Yock, and P. J. Fitzgerald, "Feasibility of a Novel Blood Noise Reduction Algorithm to Enhance Reproducibility of Ultra-High-Frequency Intravascular Ultrasound Images," *Circulation*, vol. 102, no. 14, pp. 1657-1663, Oct.2000.

[72] I. Fontaine, D. Savery, and G. Cloutier, "Simulation of Ultrasound Backscattering by Red Cell Aggregates: Effect of Shear Rate and Anisotropy," *Biophys. J.*, vol. 82, no. 4, pp. 1696-1710, Apr.2002.

[73] W. Shyh-Hau and K. K. Shung, "In vivo measurements of ultrasonic backscattering in blood," *Ultrasonics, Ferroelectrics and Frequency Control, IEEE Transactions on*, vol. 48, no. 2, pp. 425-431, 2001.

[74] M. S. van der Heiden, M. G. M. de Kroon, N. Bom, and C. Borst, "Ultrasound backscatter at 30 MHz from human blood: Influence of rouleau size affected by blood modification and shear rate," *Ultrasound in Medicine & Biology*, vol. 21, no. 6, pp. 817-826, 1995.

[75] W. Shyh-Hau and K. K. Shung, "An approach for measuring ultrasonic backscattering from biological tissues with focused transducers," *Biomedical Engineering, IEEE Transactions on*, vol. 44, no. 7, pp. 549-554, 1997.

[76] R. H. Peter, "Physical Properties of Tissues Relevant to Arterial Ultrasound Imaging and Blood Velocity Measurement,", 33 ed 2007, pp. 1527-1539.

[77] Merrill EW, "Rheology of blood.," *Physiol. Rev.*, vol. 49, pp. 863-888, 1969.

[78] Caro C.G., Pedley T.J, Schroter R.C, and Seed W.A., *The Mechanics of the Circulation*. Oxford: Oxford University Press, 1978, pp. 176-180.

[79] Chien S., "Shear dependence of effective cell volume as determinant of blood viscosity," *Science*, no. 168, pp. 977-979, 1970.

[80] Morse P.M. and Ingard K.U, *Theoretical acoustics*. Princeton, NJ: Princeton University Press, 1987.

[81] F. A. K. W. F. D. Borders SE, "Ultrasonic energy backscattered from blood—Experimental-determination of variation of sound energy with hematocrit," *Annals of Biomedical Engineering*, vol. 6, pp. 83-92, 1978.

[82] S. KK. Yuan YW, "Ultrasonic backscatter from flowing wholeblood. 2. Dependence on frequency and fibrinogen concentration.," *Acoustic Society of America*, vol. 84, pp. 1195-1200, 1988.

[83] B. Sigel, J. Machi, J. C. Beitler, J. Justin, and J. C. Coelho, "Variable ultrasound echogenicity in flowing blood," *Science*, vol. 218, no. 4579, pp. 1321-1323, Dec.1982.

[84] S. KK. Yuan YW, "Ultrasonic backscatter from flowing wholeblood.1. Dependence on shear rate and hematocrit," *Acoustic Society of America*, vol. 84, pp. 52-58, 1988.

[85] K. K. Shung, G. Cloutier, and C. C. Lim, "The effects of hematocrit, shear rate, and turbulence on ultrasonic Doppler spectrum from blood," *Biomedical Engineering, IEEE Transactions on*, vol. 39, no. 5, pp. 462-469, 1992.

[86] K. I. S. K. C. L. C. R. Mo LYL, "Ultrasound scattering from blood with hematocrits up to 100%," *IEEE Transaction in Biomedical Engineering*, vol. 41, pp. 91-95, 1994.

[87] S. B. M. J. F. E. S. J. K. A. J. J. Kitamura H, "Roles of hematocrit and fibrinogen in red-cell aggregation determined by ultrasonic scattering properties.," *Ultrasound in Medicine & Biology*, vol. 21, pp. 827-832, 1995.

[88] S. K. Wu SJ, "An in vitro study of the effects of Doppler angle, fibrinogen, and hematocrit on ultrasonic Doppler power," *IEEE Transaction in Ultrasound, Ferreoelectronics, and Frequency Control*, vol. 46, pp. 197-204, 1999.

[89] S. J. Wu and K. K. Shung, "Cyclic variation of Doppler power from whole blood under pulsatile flow,", 22 ed 1995, pp. 883-894.

[90] R. C. J. Y. T.-J. T. L. T. T. Wenguang Li, "Multi-Frequency Processing for Lumen Enhancement with Wideband Intravascular Ultrasound," *manuscript submitted to Ultrasonics Symposium IEEE 2008*, Nov.2008.

[91] V. R. Kumar, K. N. Dariush, R. H. Peter, and L. Jaap, "Validation of a New Blood-Mimicking Fluid for Use in Doppler Flow Test Objects,", 24 ed 1998, pp. 451-459.

[92] Frank M.White, *Fluid Mechanics*, 5th ed. New York: McGraw-Hill, 2005.

[93] William Nichols and Michael F.O'Rourke, *McDonald's Blood Flow in Arteries: Theoretical, Experimental, and Clinical*, 4th ed. London: Arnold, 1998.

[94] J. R. Yuan, X. Jiang, Pei-Jie Cao, A. Sadaka, R. Bautista, K. Snook, and P. W. Rehrig, "5C-5 High Frequency Piezo Composites Microfabricated Ultrasound Transducers for Intravascular Imaging," *Ultrasonics Symposium, 2006. IEEE*, pp. 264-268, Oct.2006.

[95] G. Pasterkamp, M. S. van der Heiden, M. J. Post, B. M. Ter Haar Romeny, W. P. Mali, and C. Borst, "Discrimination of the intravascular lumen and dissections in a single 30-MHz US image: use of "confounding" blood backscatter to advantage," *Radiology*, vol. 187, no. 3, pp. 871-872, June1993.

[96] W. Li, A. F. W. van der Steen, C. T. Lancee, J. Honkoop, E. J. Gussenhoven, and N. Bom, "Temporal correlation of blood scattering signals from intravascular ultrasound,", 2 ed 1995, pp. 1515-1518.

[97] R. J. Siegel, M. Ariani, M. C. Fishbein, J. S. Chae, J. C. Park, G. Maurer, and J. S. Forrester, "Histopathologic validation of angioscopy and intravascular ultrasound," *Circulation*, vol. 84, no. 1, pp. 109-117, July1991.